JCI The Journal of Clinical Investigation

Inactivation of endothelial ZEB1 impedes tumor progression and sensitizes tumors to conventional therapies

Rong Fu, … , Tao Lu, Zhao-Qiu Wu

J Clin Invest. 2020;130(3):1252-1270. https://doi.org/10.1172/JCI131507.

Research Article | Angiogenesis | Therapeutics

Graphical abstract

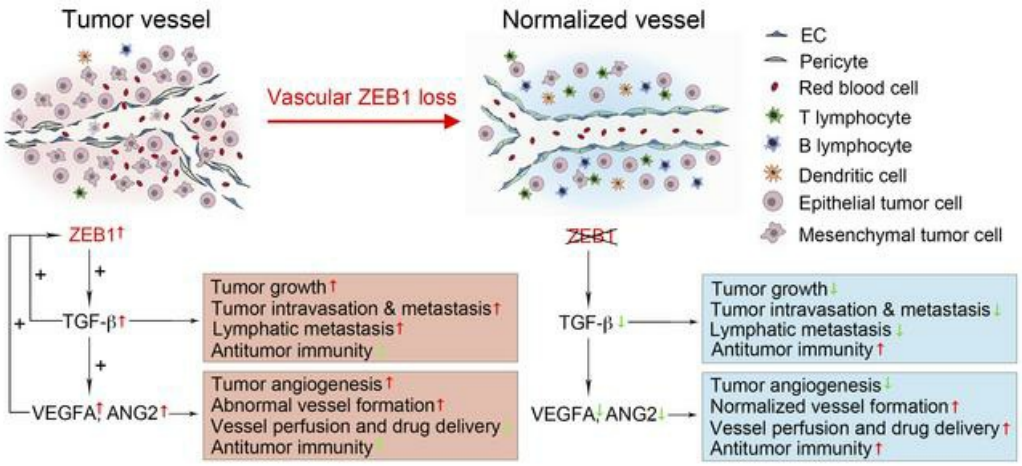

Inactivation of endothelial ZEB1 impedes tumor progression and sensitizes tumors to conventional therapies

Rong Fu,[1] Yi Li,[1] Nan Jiang,[1] Bo-Xue Ren,[1] Chen-Zi Zang,[1] Li-Juan Liu,[1] Wen-Cong Lv,[1] Hong-Mei Li,[2] Stephen Weiss,[3] Zheng-Yu Li,[4] Tao Lu,[2] and Zhao-Qiu Wu[1]

[1]State Key Laboratory of Natural Medicines, School of Basic Medicine and Clinical Pharmacy, China Pharmaceutical University, Nanjing, China. [2]State Key Laboratory of Natural Medicines, Laboratory of Molecular Design and Drug Discovery, School of Science, China Pharmaceutical University, Nanjing, China. [3]Life Sciences Institute, Rogel Cancer Center, Department of Internal Medicine, Michigan Medicine, University of Michigan, Ann Arbor, Michigan, USA. [4]Department of Medicinal Chemistry, College of Chemistry, University of Glasgow, Glasgow, United Kingdom.

Current antiangiogenic therapy is limited by its cytostatic property, scarce drug delivery to the tumor, and side toxicity. To address these limitations, we unveiled the role of ZEB1, a tumor endothelium–enriched zinc-finger transcription factor, during tumor progression. We discovered that the patients who had lung adenocarcinomas with high ZEB1 expression in tumor endothelium had increased prevalence of metastases and markedly reduced overall survival after the diagnosis of lung cancer. Endothelial ZEB1 deletion in tumor-bearing mice diminished tumor angiogenesis while eliciting persistent tumor vascular normalization by epigenetically repressing TGF-β signaling. This consequently led to improved blood and oxygen perfusion, enhanced chemotherapy delivery and immune effector cell infiltration, and reduced tumor growth and metastasis. Moreover, targeting vascular ZEB1 remarkably potentiated the anticancer activity of nontoxic low-dose cisplatin. Treatment with low-dose anti–programmed cell death protein 1 (anti–PD-1) antibody elicited tumor regression and markedly extended survival in ZEB1-deleted mice, conferring long-term protective anticancer immunity. Collectively, we demonstrated that inactivation of endothelial ZEB1 may offer alternative opportunities for cancer therapy with minimal side effects. Targeting endothelium-derived ZEB1 in combination with conventional chemotherapy or immune checkpoint blockade therapy may yield a potent and superior anticancer effect.

Introduction

The vasculature of solid tumors is structurally abnormal relative to that of nonmalignant tissues, characterized by highly permeable and leaky vessels, enhanced angiogenic sprouting, and loss of hierarchical architecture (1–4). This structural abnormality of tumor vessels impairs perfusion and oxygenation, and the resulting hypoxia and acidosis promote tumor growth, progression, and treatment resistance (5–7). In addition, the leaky nature of tumor vessels facilitates an extravasation of blood components into the surrounding interstitial space, resulting in spontaneous hemorrhages and increased interstitial fluid pressure in the tumor microenvironment (TME) (5, 6). Tumor hypoxia, together with hypoperfusion and elevated interstitial fluid pressure, impedes the delivery of therapeutic agents and immune effector cells to the tumor parenchyma, thus hindering their anticancer activity (8, 9). Tumor vessel normalization, which involves partial pruning of the immature vessels and remodeling of the remaining vessels, has therefore gained interest as a therapeutic strategy to improve penetration of anticancer drugs and immune effector cells and thus enhance the outcome of chemotherapy and immunotherapy (1, 4, 5, 9).

Traditional antiangiogenic strategies mainly focus on blocking tumor blood supply to inhibit tumor growth (6, 10, 11). However, these approaches often induce tumor hypoxia by excessively pruning vessels or forming dysfunctional vessels, and eventually lead to increased local invasion and distant metastasis (12–14). Although transient vessel normalization has been demonstrated in a variety of cancer models, creation of persistent normalization by current antiangiogenic approaches is still impossible, which significantly limits their efficacy (15). Importantly, current antiangiogenic approaches are more toxic than expected, particularly when used in combination with cytotoxic agents (16–18). Thus, the designing of an alternative strategy that can circumvent the shortcomings of current antiangiogenic therapies is highly desirable.

The zinc-finger transcription factor ZEB1 is most frequently characterized as an important driver of tumor invasion, metastasis, and treatment resistance by inducing epithelial-mesenchymal transition (EMT) in the in vitro–cultured tumor cells (19–23). However, by examining tumor samples of various human cancer types, including breast, pancreatic, and colorectal cancers, other investigators have demonstrated that ZEB1 is predominantly expressed in the tumor stromal compartment but essentially absent in the tumor epithelial compartment (24–27). It remains elusive whether ZEB1 induces cell-autonomous effects in tumor

Authorship note: RF, YL, NJ, and BXR share first authorship.
Conflict of interest: The authors have declared that no conflict of interest exists.

Submitted: July 3, 2019; **Accepted:** December 3, 2019; **Published:** February 10, 2020.
Reference information: *J Clin Invest*. 2020;130(3):1252–1270.
https://doi.org/10.1172/JCI131507.

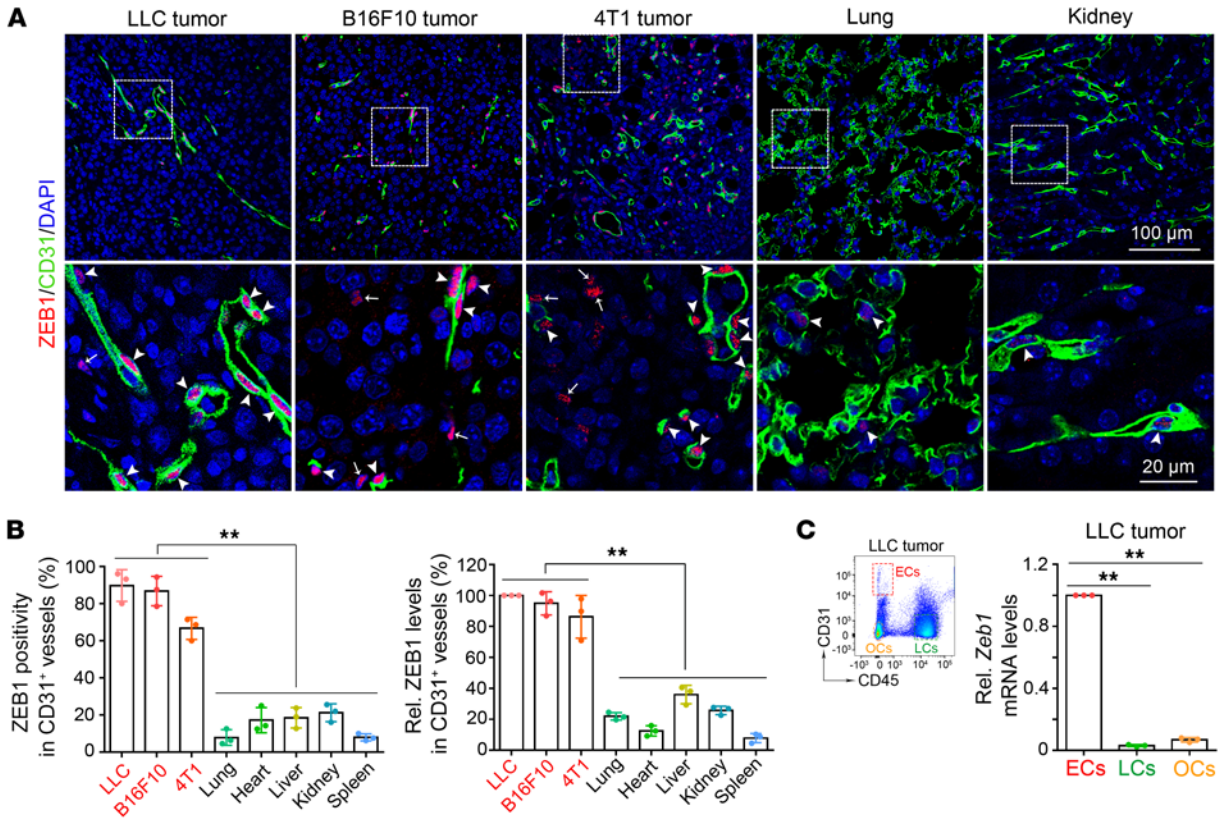

Figure 1. Endothelial ZEB1 expression is enhanced in various mouse tumor models. (**A**) Immunofluorescent images showing ZEB1 expression in CD31$^+$ blood vessels of transplanted LLC, B16F10, and 4T1 tumors, and lung and kidney tissues (3 mice each). Magnified areas of dashed boxed sections are shown in bottom panels. Arrowheads show ZEB1$^+$CD31$^+$ ECs, and arrows indicate ZEB1$^+$CD31$^-$ non-ECs. Nuclei, DAPI (blue). (**B**) Comparisons of ZEB1 positivity (left) and expression levels (right) in CD31$^+$ blood vessels of transplanted tumors versus normal tissues as shown in **A** (n = 3 independent experiments). (**C**) Comparison of *Zeb1* mRNA expression in FACS-isolated CD31$^+$CD45$^-$ ECs, CD31$^-$CD45$^+$ leukocytes (LCs), and CD31$^-$CD45$^-$ other cells (OCs) of LLC tumors (n = 3 independent experiments). Representative flow cytometric plot is shown in left panel. All data are represented as mean ± SD. $^{**}P < 0.01$. Differences were tested using 1-way ANOVA with Tukey's post hoc test.

stromal endothelial cells (ECs) and whether this has an impact on tumor progression and metastasis. Here, we investigate the vascular expression pattern of ZEB1 in malignant tumors versus normal tissues in humans and mice, and study the biological and therapeutic relevance of selectively targeting ZEB1 to tumor angiogenesis, vascular normalization, tumor progression and metastasis, and tumor response to conventional chemotherapy and immune checkpoint blockade therapy. Meanwhile, we pursue a mechanistic understanding of how inactivation of EC-derived ZEB1 affects tumor progression and response to these therapeutic approaches.

Results

Vascular ZEB1 levels are increased in various tumors and correlate negatively with survival rates in lung cancer patients. To examine ZEB1 expression in tumor tissues, we employed the ectopic Lewis lung carcinoma (LLC) and B16F10 tumor models by subcutaneously implanting LLC and B16F10 melanoma cells into adult C57BL/6 male or female mice, and the orthotopic 4T1 tumor model by orthotopically injecting 4T1 breast carcinoma cells into the fat pads of adult C57BL/6 females. These tumor cells did not express *Zeb1* mRNA or protein either in culture (Supplemental Figure 1, A and B; supplemental material available online with this article; https://doi.org/10.1172/JCI131507DS1) or upon tumor formation in mice (Supplemental Figure 1C). Intriguingly, ZEB1 expression was mainly confined to CD31$^+$ tumor ECs in ectopic LLC and B16F10 tumors and orthotopic 4T1 tumors, only occasionally present in some non-ECs within the tumor microenvironment (TME) (Figure 1, A and B, and Supplemental Figure 1C). Furthermore, quantitative reverse transcriptase PCR (qRT-PCR) analysis of FACS-isolated cells from LLC tumors showed that *Zeb1* transcript was predominantly expressed in CD31$^+$CD45$^-$ tumor ECs, with a weak expression in CD31$^-$CD45$^-$ cells (e.g., vascular pericytes and fibroblasts) but no expression in CD31$^-$CD45$^+$ tumor-infiltrating leukocytes (Figure 1C). In addition, immunofluorescence analyses of ZEB1 and CD45 in the LLC tumor further confirmed that ZEB1 expression was largely absent in CD45$^+$ leukocytes (Supplemental Figure 1D). In contrast to robust expression in tumor ECs, ZEB1 expression in normal tissues of adult mice was very infrequent and indistinct, exhibiting remarkably lower ZEB1 positivity and reduced expression levels in comparison with tumor vessels (Figure 1, A and B, and Supplemental Figure 1E).

To unveil the relevance of ZEB1 in human tumor angiogenesis and progression, we compared ZEB1 expression in human lung carcinoma tissues versus adjacent normal tissues. We discovered that vascular ZEB1 expression levels in human lung adenocarcinomas were significantly higher than those in adjacent normal

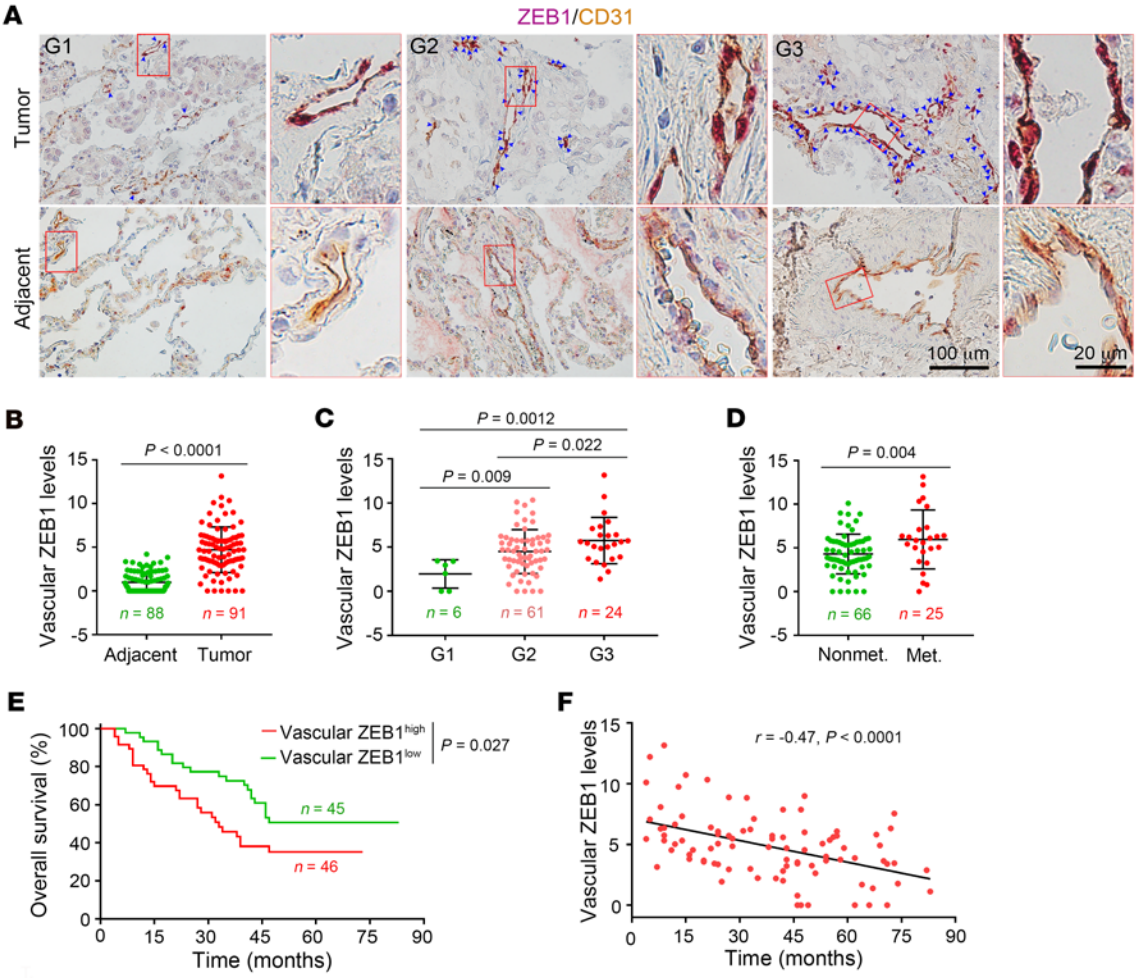

Figure 2. Vascular ZEB1 expression correlates negatively with survival rates in lung cancer patients. (**A**) Representative examples of ZEB1 (red) and CD31 (brown) immunohistochemical staining of human lung cancer tissue arrays (n = 91) and matched adjacent normal samples (n = 88). Magnified areas of red boxed sections are shown in right panels. Arrowheads show ZEB1$^+$ tumor ECs. (**B**) Comparison of vascular ZEB1 expression in lung cancer tissues versus matched adjacent normal tissues as described in **A**. (**C**) Comparison of vascular ZEB1 expression in lung cancer tissues with different pathological gradings as described in **A**. (**D**) Comparison of vascular ZEB1 expression in lung cancer tissues of patients with metastases versus patients without metastases as described in **A**. (**E**) Kaplan-Meier survival analysis of the relationship between overall survival rate and vascular ZEB1 expression in lung cancer patients as described in **A**. The cutoff value is the average vascular ZEB1 expression level of all patients. (**F**) Correlation plot between vascular ZEB1 expression and lung cancer patient survival time. All data are represented as mean ± SD. Differences were tested using unpaired 2-tailed Student's t test (**B** and **D**), 1-way ANOVA with Tukey's post hoc test (**C**), log-rank test (**E**), and 2-tailed Pearson test (**F**).

tissues, and its levels were remarkably increased upon tumor progression, as assessed by immunohistochemistry (Figure 2, A–C) and immunofluorescence (Supplemental Figure 1F). Furthermore, we found that the patients who had lung adenocarcinomas with high ZEB1 expression in tumor vessels had increased prevalence of local or distal metastases (Figure 2D) and markedly reduced overall survival after the diagnosis of lung cancer (Figure 2E). Consistently, we noted an inverse relationship between vascular ZEB1 levels and overall survival in patients with lung adenocarcinoma (Figure 2F). Taken together, these results suggest that ZEB1 is predominantly expressed in tumor vessels, and its levels positively correlate with human cancer progression.

ZEB1 deletion in tumor ECs reduces tumor growth, intravasation, and metastasis in various cancer models. To address the potential role of vascular ZEB1 in normal tissues of adult mice, we generated inducible EC-specific *Zeb1* conditional knockout mice (designated $Zeb1^{i\Delta EC}$) by mating $Zeb1^{fl/fl}$ mice (mice were generated and maintained in our laboratory) with $Cdh5\text{-}Cre^{ERT2}$ transgenics (28) (Supplemental Figure 2, A–C). To induce Cre activity and vascular *Zeb1* inactivation, 8-week-old adult male or female mice were intraperitoneally injected with 1.0 mg tamoxifen every other day for 2 consecutive weeks (Supplemental Figure 2, D and E). Notably, there were no differences in vascular morphology and density between $Zeb1^{i\Delta EC}$ mice and $Zeb1^{WT}$ mice ($Zeb1^{fl/fl}$) (Supplemental Figure 2, E and F). Also, $Zeb1^{i\Delta EC}$ mice grew normally without any growth retardation or detectable histological alterations in major organs including lung, heart, liver, and kidney (Supplemental Figure 2G). To further study the potential role of endothelial ZEB1 in retinal angiogenesis, mice were treated with 0.1 mg tamoxifen at postnatal day 3 (P3) and P6, and retinas were dissected at P7 for whole-mount immunofluorescent staining (Supplemental Figure 2H). As in normal tissues of adult

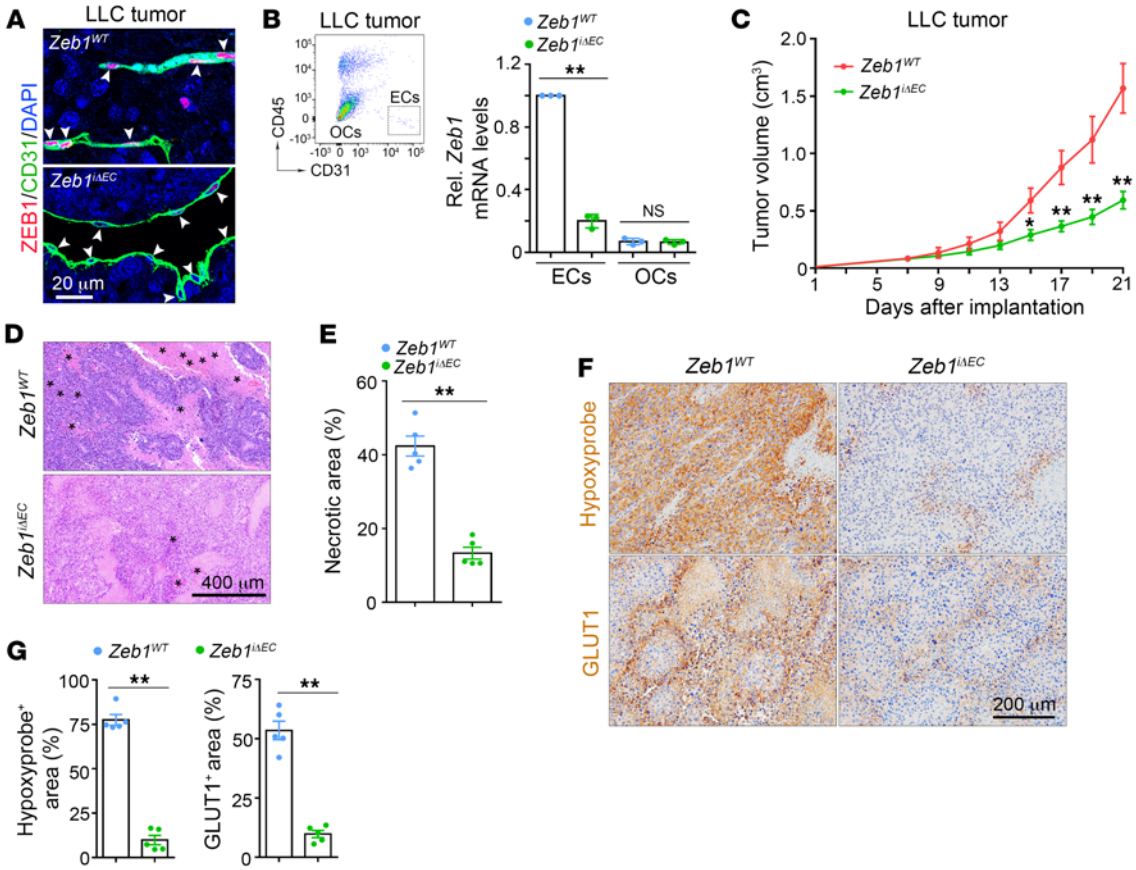

Figure 3. Vascular ZEB1 deficiency inhibits LLC tumor growth. (**A**) Immunofluorescent images showing ZEB1 expression in CD31$^+$ blood vessels of LLC tumors grown in *Zeb1*^{WT} but not *Zeb1*$^{i\Delta EC}$ mice (3 mice each). Arrowheads show ZEB1$^+$ or ZEB1$^-$ tumor ECs. Nuclei, DAPI (blue). (**B**) Comparison of *Zeb1* mRNA expression in FACS-isolated ECs and OCs of LLC tumors grown in *Zeb1*^{WT} versus *Zeb1*$^{i\Delta EC}$ mice (n = 3 independent experiments). Representative flow cytometric plot is shown in left panel. (**C**) Comparison of growth curves of LLC tumors grown for 21 days in *Zeb1*^{WT} versus *Zeb1*$^{i\Delta EC}$ mice (5 mice each). (**D** and **E**) H&E-stained images (**D**) and quantification (**E**) of hemorrhagic necrosis in LLC tumors of *Zeb1*^{WT} versus *Zeb1*$^{i\Delta EC}$ mice (5 mice each). Asterisks mark hemorrhagic foci. (**F** and **G**) Immunohistochemical images (**F**) and comparisons (**G**) of hypoxyprobe-1$^+$ and GLUT1$^+$ areas in LLC tumors of *Zeb1*^{WT} versus *Zeb1*$^{i\Delta EC}$ mice (5 mice each). All data are represented as mean ± SD. $^*P < 0.05$; $^{**}P < 0.01$. Differences were tested using unpaired 2-sided Student's t test (**B**, **E**, and **G**) and 2-way ANOVA with Tukey's post hoc test (**C**).

mice, ZEB1 expression in retinal ECs was very infrequent and indistinct (Supplemental Figure 2I). Although ZEB1 expression in retinal ECs was efficiently depleted, defects in retinal angiogenesis were not detected (Supplemental Figure 2, I–K). Taken together, these results suggest that ZEB1 is a potential candidate for vascular-targeted therapy with attenuated systemic adverse effects compared with current antiangiogenic approaches.

To define the role of vascular ZEB1 in tumor progression, we evaluated LLC and B16F10 tumor models by subcutaneous implantation of LLC and B16F10 cells into 9-week-old *Zeb1*^{WT} and *Zeb1*$^{i\Delta EC}$ mice that were intraperitoneally injected with 1.0 mg tamoxifen every other day for 2 consecutive weeks starting from 1 week before tumor implantation. Also, we used an orthotopic Panc02 tumor model by orthotopically injecting Panc02 pancreatic carcinoma cells into the head of pancreas in 9-week-old *Zeb1*^{WT} and *Zeb1*$^{i\Delta EC}$ mice (29). We confirmed that ZEB1 expression was efficiently deleted in tumor ECs in LLC, B16F10, and Panc02 tumors of *Zeb1*$^{i\Delta EC}$ mice compared with *Zeb1*^{WT} mice (Figure 3, A and B, and Supplemental Figure 3, A and J). At 3 weeks after implantation, LLC, B16F10, and Panc02 tumors showed 62%, 64%, and 67% reduced growth in *Zeb1*$^{i\Delta EC}$ mice, respectively, in comparison with *Zeb1*^{WT} mice (Figure 3C and Supplemental Figure 3, B and K). Notably, LLC and B16F10 tumors showed significantly reduced intratumoral hemorrhagic necrosis in *Zeb1*$^{i\Delta EC}$ mice compared with *Zeb1*^{WT} mice, indicating slower growth rates in *Zeb1*$^{i\Delta EC}$ tumors (Figure 3, D and E, and Supplemental Figure 3, C and D). Moreover, staining for the hypoxia markers pimonidazole and glucose transporter 1 (GLUT1) revealed a reduced hypoxic tumor area in *Zeb1*$^{i\Delta EC}$ mice compared with *Zeb1*^{WT} mice (Figure 3, F and G, and Supplemental Figure 3, E and F), suggesting that LLC and B16F10 tumors of *Zeb1*$^{i\Delta EC}$ mice were better oxygenated, which in turn reduced tumor necrosis.

In most tumors, EMT is accompanied by hypoxia. Immunofluorescent staining of LLC tumors revealed remarkably increased expression of E-cadherin (a classic epithelial marker) in tandem with a reduction in expression of vimentin (a mesenchymal marker) in *Zeb1*$^{i\Delta EC}$ mice compared with *Zeb1*^{WT} mice (Figure 4, A and B), indicating that the EMT process was significantly hindered in *Zeb1*$^{i\Delta EC}$ tumors. As tumor hypoxia and EMT are known to promote tumor metastasis and are indicative of poor prognosis

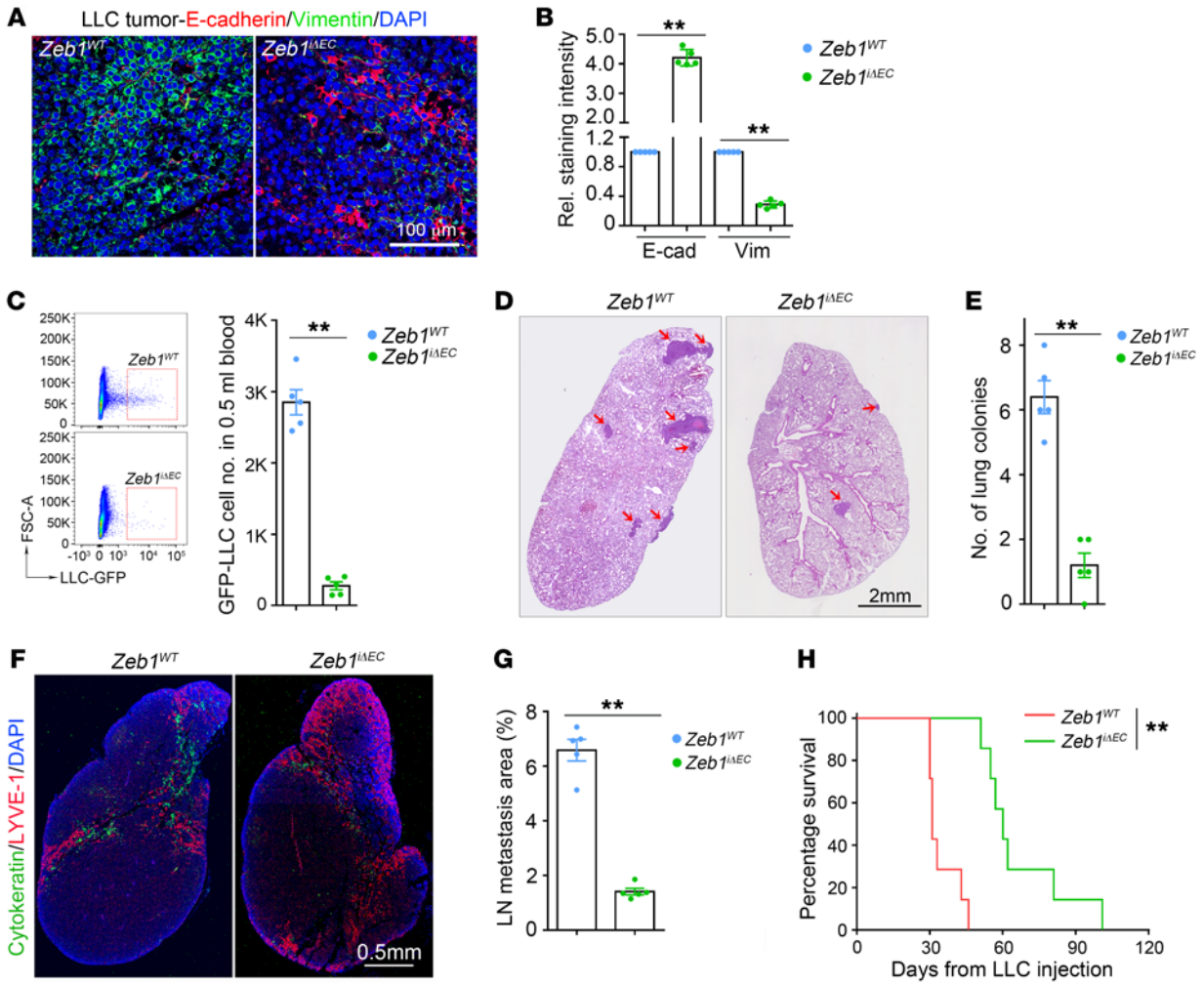

Figure 4. Endothelial ZEB1 deletion impedes LLC tumor intravasation and metastasis. (**A** and **B**) Immunofluorescent images (**A**) and comparisons (**B**) of E-cadherin and vimentin expression in LLC tumors of *Zeb1*^{WT} versus *Zeb1*$^{i\Delta EC}$ mice (5 mice each). (**C**) Comparison of numbers of circulating GFP-LLC cells in tumor-bearing *Zeb1*^{WT} versus *Zeb1*$^{i\Delta EC}$ mice (5 mice each). (**D** and **E**) H&E-stained images (**D**) and comparison (**E**) of metastatic colonies in lungs of tumor-bearing *Zeb1*^{WT} versus *Zeb1*$^{i\Delta EC}$ mice (5 mice each). Arrows denote metastatic foci. (**F** and **G**) Immunofluorescent images (**F**) and comparison (**G**) of metastasized cytokeratin$^+$ LLC tumor cells in the inguinal LNs of tumor-bearing *Zeb1*^{WT} versus *Zeb1*$^{i\Delta EC}$ mice (5 mice each). The cytokeratin$^+$ area is presented as a percentage of sectional area. (**H**) Comparison of overall survival of LLC tumor–bearing *Zeb1*^{WT} versus *Zeb1*$^{i\Delta EC}$ mice (5 mice each). All data are represented as mean ± SD. $^{**}P < 0.01$. Differences were tested using unpaired 2-sided Student's *t* test (**B**, **C**, **E**, and **G**) and log-rank test (**H**).

(30), we compared tumor intravasation and metastasis in *Zeb1*^{WT} versus *Zeb1*$^{i\Delta EC}$ mice. To monitor tumor intravasation, mice were implanted with GFP-labeled LLC cells, and circulating nucleated cells were isolated 3 weeks after tumor implantation for flow cytometric analysis. The results demonstrated a smaller number of GFP$^+$ circulating tumor cells in *Zeb1*$^{i\Delta EC}$ mice than in *Zeb1*^{WT} mice (Figure 4C), suggesting that endothelial ZEB1 deletion significantly diminished tumor cell intravasation. To address the role of vascular ZEB1 in tumor cell metastasis, mice were implanted with LLC cells, and lungs and inguinal lymph nodes (LNs) were collected 4 weeks and 3 weeks after tumor implantation, respectively. We observed that the number of metastatic tumor colonies in the lungs was 80% less in *Zeb1*$^{i\Delta EC}$ mice (Figure 4, D and E). Although the distribution and densities of lymphatic vessels in LLC tumors and inguinal LNs were largely comparable in *Zeb1*$^{i\Delta EC}$ and *Zeb1*^{WT} mice (Supplemental Figure 3, G and H), lymphatic metastasis of LLC cells into inguinal LNs was remarkably impeded by nearly 80% in *Zeb1*$^{i\Delta EC}$ mice (Figure 4, F and G). Moreover, overall survival of *Zeb1*$^{i\Delta EC}$ mice carrying LLC and B16F10 tumors was profoundly increased in comparison with tumor-bearing *Zeb1*^{WT} mice (Figure 4H and Supplemental Figure 3I). Altogether, these data suggest that endothelial ZEB1 deletion reduces tumor cell growth, intravasation, distant metastasis, and lymphatic metastasis, thereby increasing survival of tumor-bearing mice.

Endothelial ZEB1 deletion reduces tumor angiogenesis while inducing tumor vessel normalization in various tumor models. To assess the impact of endothelial ZEB1 deletion on tumor angiogenesis, we measured vessel density in tumor tissues 3 weeks after implantation. As shown, LLC, B16F10, and Panc02 tumors of *Zeb1*$^{i\Delta EC}$ mice exhibited a reduced number of vessels in comparison with *Zeb1*^{WT} mice, indicating that endothelial ZEB1 deletion profoundly reduced tumor angiogenesis (Figure 5A and

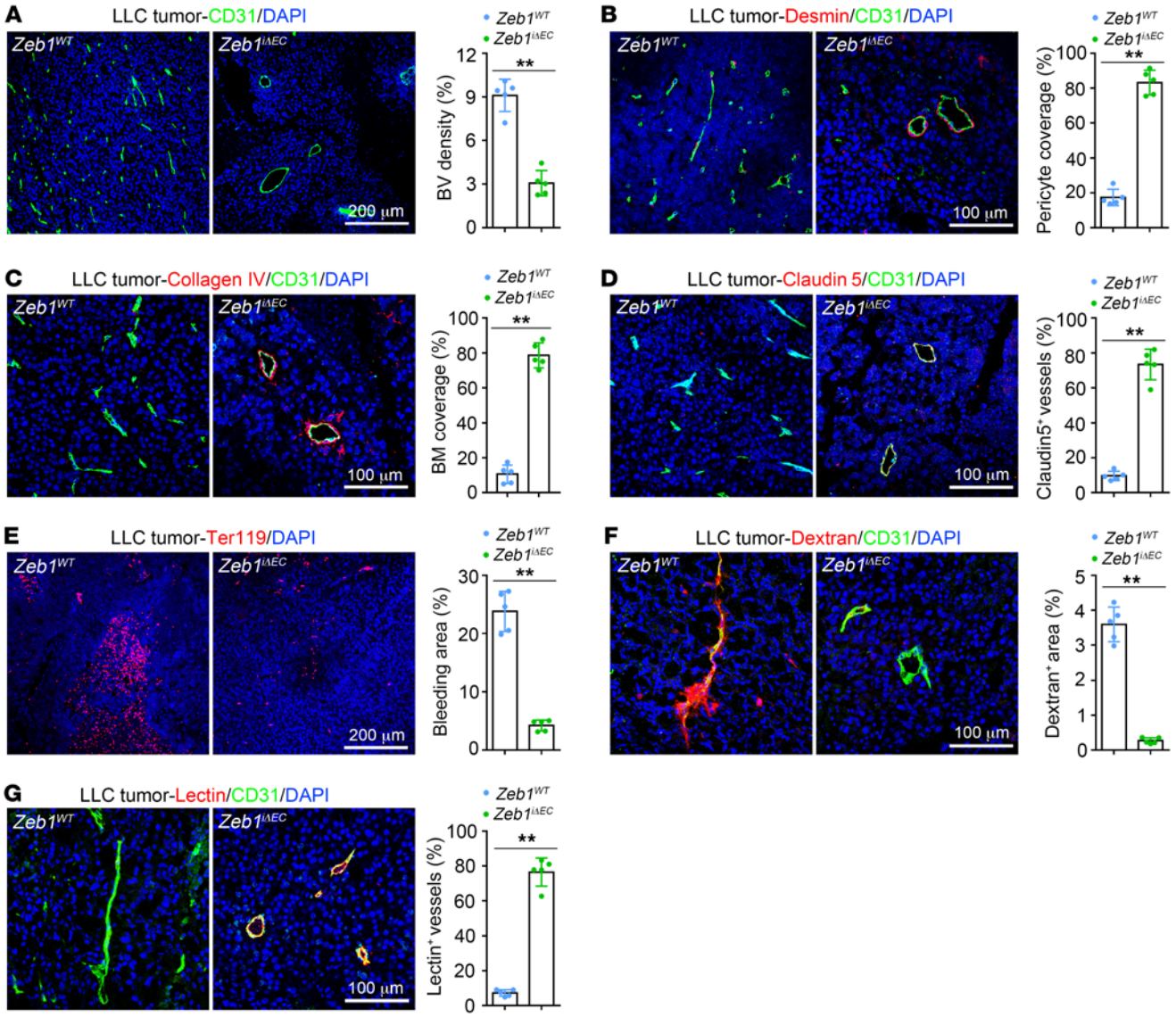

Figure 5. Endothelial ZEB1 inactivation reduces LLC tumor angiogenesis while eliciting vessel normalization. (**A**) Immunofluorescent images (left) and comparison (right) of CD31$^+$ blood vessel (BV) density in LLC tumors grown for 21 days in *Zeb1*^{WT} versus *Zeb1*$^{i\Delta EC}$ mice (5 mice each). Nuclei, DAPI (blue). (**B**–**D**) Immunofluorescent images (left) and comparisons (right) of desmin$^+$ pericyte coverage along BVs (**B**), collagen type IV$^+$ basement membrane (BM) coverage alongside BVs (**C**), and claudin 5 distribution on BVs (**D**) in LLC tumors of *Zeb1*^{WT} versus *Zeb1*$^{i\Delta EC}$ mice (5 mice each). (**E**) Immunofluorescence images (left) and comparison (right) of extravasated Ter119$^+$ red blood cells in LLC tumors of *Zeb1*^{WT} versus *Zeb1*$^{i\Delta EC}$ mice (5 mice each). The Ter119$^+$ bleeding area is presented as a percentage of total sectional area. (**F** and **G**) Immunofluorescent images (left) and comparisons (right) of dextran leakage (**F**) and lectin perfusion (**G**) of BVs in LLC tumors of *Zeb1*^{WT} versus *Zeb1*$^{i\Delta EC}$ mice (5 mice each). Dextran and lectin were intravenously injected 30 minutes before euthanization. The dextran$^+$ area or lectin$^+$ vessels are presented as a percentage of total sectional area or CD31$^+$ area, respectively. All data are represented as mean ± SD. $^{**}P < 0.01$. Differences were tested using unpaired 2-sided Student's *t* test.

Supplemental Figure 4, A and H). Next, we assessed the role of endothelial ZEB1 in vascular integrity and function. We found that desmin$^+$ pericyte coverage along tumor vessels, collagen type IV$^+$ basement membrane (BM) coverage, and distribution of the endothelial junctional molecule claudin 5 on tumor vessels were markedly increased in LLC, B16F10, and Panc02 tumors of *Zeb1*$^{i\Delta EC}$ mice (Figure 5, B–D, and Supplemental Figure 4, B–D, I, and J), suggesting that endothelial ZEB1 deletion efficiently promotes tumor vessel integrity. Consistently, *Zeb1*$^{i\Delta EC}$ tumor vessels showed reduced intratumoral hemorrhages (assessed by Ter119 staining for red blood cells) and lower tumor vascular permeability to intravenously injected 70-kDa dextran, thus implicating endothelial ZEB1 in tumor vascular leakiness (Figure 5, E and F, and Supplemental Figure 4, E and F). Further, we evaluated tumor vascular functionality by intravenously injecting fluorescently labeled lectin. Tumor vascular perfusion was markedly promoted in tumors of *Zeb1*$^{i\Delta EC}$ mice compared with *Zeb1*^{WT} mice (Figure 5G and Supplemental Figure 4G). To unveil the role of vascular ZEB1 in early tumor progression, we measured vessel density and integrity in LLC tumors 1 week after implantation. We confirmed that ZEB1 was indeed expressed in tumor ECs, and its expression in tumor ECs was efficiently deleted in tumors of *Zeb1*$^{i\Delta EC}$ mice that

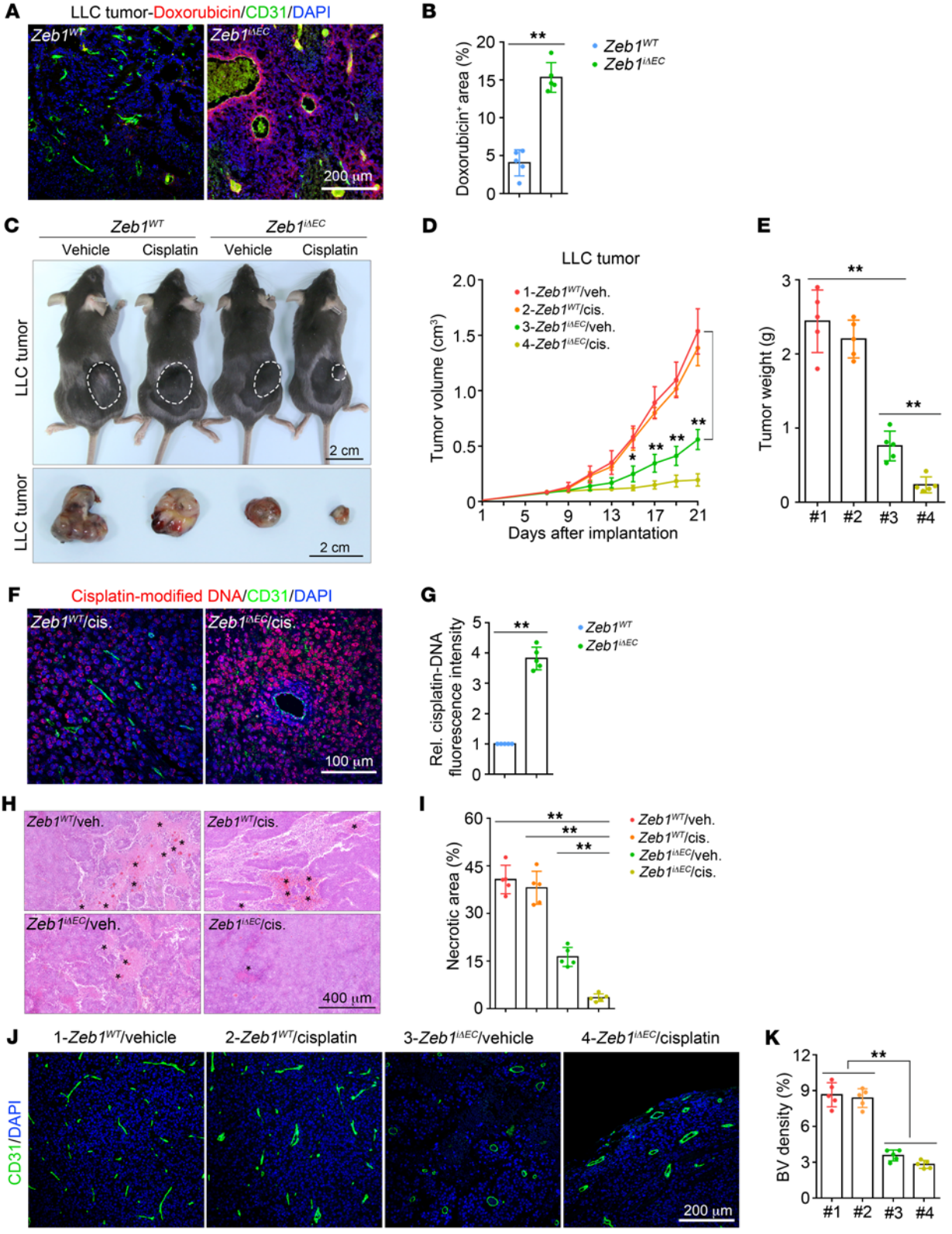
A
LLC tumor-Doxorubicin/CD31/DAPI
Zeb1WT
Zeb1iΔEC
200 μm
B
Doxorubicin+ area (%)
Zeb1WT
Zeb1iΔEC
C
Zeb1WT
Zeb1iΔEC
Vehicle
Cisplatin
LLC tumor
2 cm
D
LLC tumor
Tumor volume (cm3)
1-Zeb1WT/veh.
2-Zeb1WT/cis.
3-Zeb1iΔEC/veh.
4-Zeb1iΔEC/cis.
Days after implantation
E
Tumor weight (g)
#1
#2
#3
#4
F
Cisplatin-modified DNA/CD31/DAPI
Zeb1WT/cis.
Zeb1iΔEC/cis.
100 μm
G
Rel. cisplatin-DNA fluorescence intensity
H
Zeb1WT/veh.
Zeb1WT/cis.
Zeb1iΔEC/veh.
Zeb1iΔEC/cis.
400 μm
I
Necrotic area (%)
J
1-Zeb1WT/vehicle
2-Zeb1WT/cisplatin
3-Zeb1iΔEC/vehicle
4-Zeb1iΔEC/cisplatin
CD31/DAPI
200 μm
K
BV density (%)

Figure 6. Vascular ZEB1 depletion enhances drug delivery and potentiates antitumor effect of cisplatin. (**A** and **B**) Immunofluorescent images (**A**) and comparison (**B**) of doxorubicin penetration in the intratumoral regions of LLC tumors grown in *Zeb1*^{WT} versus *Zeb1*$^{i\Delta EC}$ mice (5 mice each). Doxorubicin was intravenously injected 15 minutes before euthanization. The doxorubicin$^+$ area is presented as a percentage of total sectional area. Nuclei, DAPI (blue). (**C** and **D**) Gross images (**C**) and growth curves (**D**) of LLC tumors grown subcutaneously for 21 days in *Zeb1*^{WT} and *Zeb1*$^{i\Delta EC}$ mice. Mice were treated with vehicle or 1 mg/kg cisplatin once every 4 days for a total of 3 times (5 mice each). (**E**) Comparison of tumor weight of the indicated LLC tumors harvested at day 21 after implantation (5 mice each). (**F** and **G**) Immunofluorescent images (**F**) and comparison (**G**) of intratumoral accumulation of cisplatin in LLC tumors of cisplatin-treated *Zeb1*^{WT} versus *Zeb1*$^{i\Delta EC}$ mice (5 mice each). (**H** and **I**) H&E-stained images (**H**) and quantification (**I**) of hemorrhagic necrosis in LLC tumors of vehicle- or cisplatin-treated *Zeb1*^{WT} and *Zeb1*$^{i\Delta EC}$ mice as described in **C** (5 mice each). Asterisks denote hemorrhagic foci. (**J** and **K**) Immunofluorescent images (**J**) and quantification (**K**) of BV density in LLC tumors of vehicle- or cisplatin-treated *Zeb1*^{WT} and *Zeb1*$^{i\Delta EC}$ mice as described in **C** (5 mice each). All data are represented as mean ± SD. $^*P < 0.05$; $^{**}P < 0.01$. Differences were tested using unpaired 2-sided Student's *t* test (**B** and **G**), 2-way ANOVA with Tukey's post hoc test (**D**), and 1-way ANOVA with Tukey's post hoc test (**E**, **I**, and **K**).

were treated with 1.0 mg tamoxifen every other day for a total of 7 times starting from 1 week before tumor inoculation (Supplemental Figure 4K). Notably, tumors grown in *Zeb1*$^{i\Delta EC}$ mice for 1 week exhibited impaired tumor vessel formation in tandem with enhanced desmin$^+$ pericyte coverage along tumor vessels (Supplemental Figure 4, K and L), indicating that vascular ZEB1 plays an essential role in early tumor progression. Taken together, these findings suggest that endothelial ZEB1 deletion reduces tumor angiogenesis while eliciting vascular normalization at different stages of tumor progression.

Vascular ZEB1 inactivation promotes chemotherapy delivery and potentiates anticancer activity of nontoxic low-dose cisplatin in the LLC tumor. Based on the findings that tumor vascular perfusion was profoundly improved in tumors of *Zeb1*$^{i\Delta EC}$ mice, we measured the accumulated amount of the chemotherapeutic agent doxorubicin in the tumor. To this end, mice were intravenously injected with 5 mg/kg doxorubicin 15 minutes before euthanization, and the tumors were dissected and subjected to immunofluorescence analysis (doxorubicin is autofluorescent, allowing direct monitoring of the drug's penetration in the tumor). Indeed, LLC tumors of *Zeb1*$^{i\Delta EC}$ mice exhibited a 3.8-fold increase in the accumulated amount of doxorubicin within perivascular areas, indicating improved delivery of a small-molecule chemotherapeutic drug in *Zeb1*$^{i\Delta EC}$ tumors (Figure 6, A and B). Thus, we sought to investigate whether vascular ZEB1 deletion can enhance tumor response to chemotherapy with low-dose cisplatin, a conventional small-molecule chemotherapeutic agent. To this end, *Zeb1*^{WT} and *Zeb1*$^{i\Delta EC}$ mice were intraperitoneally injected with vehicle or cisplatin (1 mg/kg) every 4 days for a total 3 times when tumor volume reached about 100 mm^3 (6–7 days after LLC tumor implantation). As expected, low-dose cisplatin failed to suppress LLC tumor growth in *Zeb1*^{WT} mice, while it significantly reduced tumor growth by about 90% in *Zeb1*$^{i\Delta EC}$ mice (Figure 6, C–E). Consistently, immunofluorescent staining using anti–cisplatin-modified DNA antibody (an antibody that enables the quantification of cisplatin-induced adducts on DNA) revealed a remarkable intratumoral accumulation of cisplatin in tumors of *Zeb1*$^{i\Delta EC}$ mice compared with *Zeb1*^{WT} mice (Figure 6, F and G), indicating profoundly improved delivery and perfusion of cisplatin in tumors of *Zeb1*$^{i\Delta EC}$ mice. Histological analyses revealed that low-dose cisplatin treatment did not reduce intratumoral necrosis in tumors of *Zeb1*^{WT} mice but dramatically decreased necrotic area by more than 90% in tumors of *Zeb1*$^{i\Delta EC}$ mice (Figure 6, H and I). As tumor necrosis is recognized to be a consequence of chronic cellular hypoxia in solid tumors, and associates with increased tumor cell proliferation, enhanced resistance to chemotherapy, and reduced disease-specific survival (3, 31, 32), we examined the effect of low-dose cisplatin on tumor cell proliferation and survival in *Zeb1*^{WT} and *Zeb1*$^{i\Delta EC}$ mice. As shown, we observed that low-dose cisplatin treatment significantly decreased the percentages of Ki67$^+$ proliferative cells while increasing the percentages of cleaved caspase-3$^+$ apoptotic cells in the LLC tumor grown in *Zeb1*$^{i\Delta EC}$ mice but not in *Zeb1*^{WT} mice (Supplemental Figure 5, A and B), suggesting that low-dose cisplatin reduced tumor cell proliferation and survival in *Zeb1*$^{i\Delta EC}$ mice. Notably, we observed reduced tumor vascular densities in tandem with elevated desmin$^+$ pericyte coverage and improved collagen type IV$^+$ BM coverage along blood vessels in the LLC tumors grown in low-dose cisplatin– or vehicle-treated *Zeb1*$^{i\Delta EC}$ mice compared with *Zeb1*^{WT} mice receiving treatment with cisplatin or vehicle (Figure 6, J and K, and Supplemental Figure 5, C and D). Importantly, we found that low-dose cisplatin–treated mice did not show any growth retardation or detectable histological alterations in major organs including heart, liver, spleen, and kidney (Supplemental Figure 5E). These findings demonstrate that targeting endothelial ZEB1 in combination with low-dose cisplatin may yield a significantly enhanced anticancer effect without eliciting systematic side effects.

Endothelial ZEB1 deficiency promotes antitumor immunity and sensitizes LLC tumors to immune checkpoint blockade. In addition to improving tumor oxygenation and drug delivery, vascular normalization may increase immune cell infiltration into the tumors, thus converting the intrinsically immunosuppressive TME to an immunosupportive one (9, 33–35). We therefore set up to investigate the impact of vascular ZEB1 deletion on infiltration of immune cells into tumors. Flow cytometry analyses of LLC tumors grown in *Zeb1*$^{i\Delta EC}$ mice revealed increased densities of CD8$^+$ and CD4$^+$ T cells, which are key immune effector cells in antitumor immunity (Figure 7, A and B). Notably, the presence of Tregs (CD4$^+$Foxp3$^+$), also known as immunosuppressive T cells, was instead diminished in *Zeb1*$^{i\Delta EC}$ tumors (Figure 7C). The analyses also showed that tumors grown in *Zeb1*$^{i\Delta EC}$ mice had enhanced infiltration of tumor-associated dendritic cells and tumor-associated B cells, the specialized antigen-presenting cells (APCs) in tumors that are required to initiate and sustain T cell–dependent antitumor immunity (Figure 7, D and E). Moreover, we performed CD8 immunohistochemical staining of LLC and B16F10 tumors grown in *Zeb1*^{WT} mice versus *Zeb1*$^{i\Delta EC}$ mice and found boosted infiltration of CD8$^+$ T cells into both peripheral and central regions of tumors grown in *Zeb1*$^{i\Delta EC}$ mice compared with *Zeb1*^{WT} mice (Figure 7, F and G, and Supplemental Figure 6, A and B).

It is conceivable that improving tumor vessel normalization can facilitate the infiltration and activation of immune cells, especially cytotoxic T cells, in the TME and thus enhances the effica-

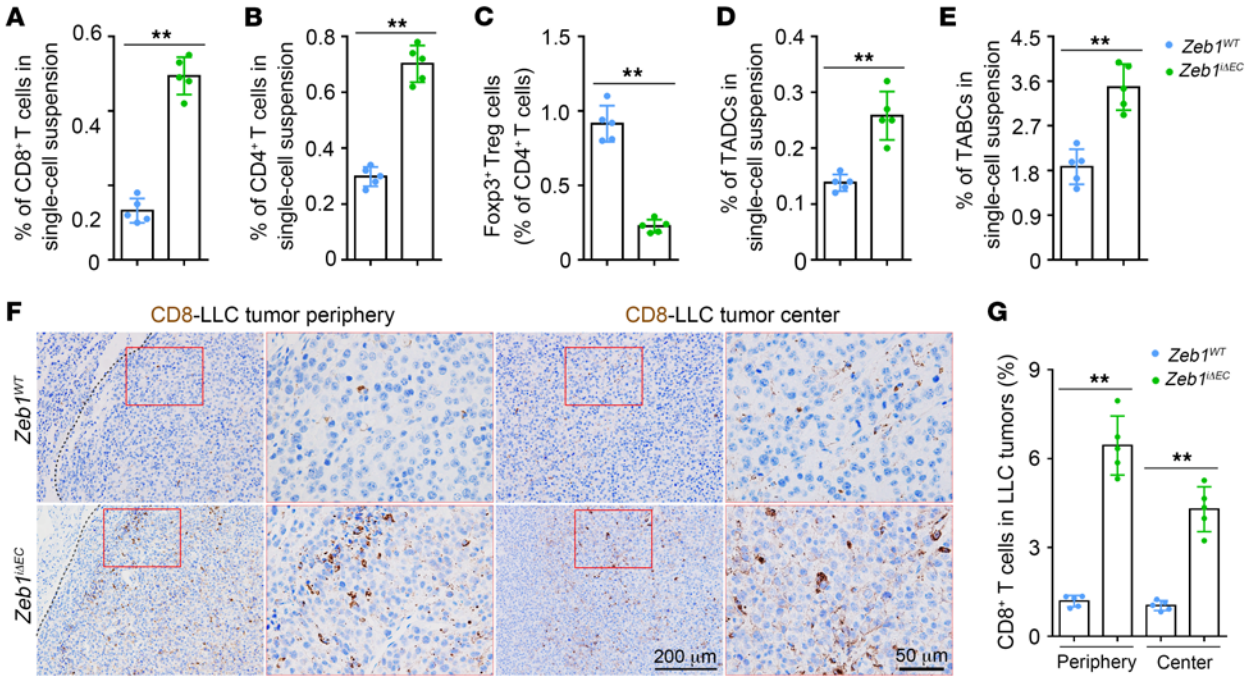

Figure 7. Endothelial ZEB1 deletion enhances presence of tumor-infiltrating immune cells. (**A**–**E**) Flow cytometric quantification of presence of CD8$^+$ T cells (**A**), CD4$^+$ T cells (**B**), CD4$^+$Foxp3$^+$ Tregs (**C**), tumor-associated dendritic cells (TADCs) (**D**), and tumor-associated B cells (TABCs) (**E**) in LLC tumors of *Zeb1*^{WT} and *Zeb1*^{iΔEC} mice (5 mice each). (**F** and **G**) Immunohistochemical images (**F**) and quantification (**G**) of CD8$^+$ T cells in the peripheral and central regions of LLC tumors grown in *Zeb1*^{WT} and *Zeb1*^{iΔEC} mice (5 mice each). Magnified areas of dashed boxed sections are shown in right panels. All data are represented as mean ± SD. $^{**}P < 0.01$. Differences were tested using unpaired 2-sided Student's *t* test (**A**–**E** and **G**).

cy of anti–programmed cell death protein 1/programmed death ligand 1 (anti–PD-1/PD-L1) immunotherapy (9, 35–37). Intriguingly, immunofluorescence analysis of the LLC tumors revealed that PD-L1 was predominantly expressed on tumor-infiltrating CD45$^+$ leukocytes with a weak expression on CD31$^+$ tumor ECs (Supplemental Figure 6C). In addition, qRT-PCR analysis of FACS-isolated cells of LLC tumors revealed that *Pdl1* mRNA expression in CD31$^-$CD45$^+$ leukocytes was 10 times and 25 times higher than that in CD31$^+$CD45$^-$ tumor ECs and CD31$^-$CD45$^-$ cells, respectively (Supplemental Figure 6D). Notably, LLC tumors of *Zeb1*^{iΔEC} mice exhibited markedly increased PD-L1 expression compared with those of *Zeb1*^{WT} mice, accompanied by enhanced presence of tumor-infiltrating CD45$^+$ leukocytes in the TME, as assessed by PD-L1/CD45 immunofluorescence (Supplemental Figure 6E). We therefore reasoned that blocking the PD-1/PD-L1 pathway may confer long-term antitumor immunity in tumor-bearing *Zeb1*^{iΔEC} mice, thus yielding potent and durable antitumor effect. To test this, 200 μg isotype control or anti–PD-1 mAb was intraperitoneally injected into *Zeb1*^{WT} and *Zeb1*^{iΔEC} mice every 3 days for a total of 3 times (around 3-fold lower than regular dose) starting when tumor volume reached 100 mm^3 (6–7 days after LLC tumor implantation). Consistent with our expectation, neither *Zeb1*^{iΔEC} mice nor *Zeb1*^{WT} mice that were treated with low-dose anti–PD-1 mAb showed any growth retardation or detectable histological alterations in major organs including heart, liver, and kidney (Supplemental Figure 6F). Treatment with low-dose anti–PD-1 mAb slightly decreased LLC tumor growth in *Zeb1*^{WT} mice (Figure 8, A and B). Most strikingly, anti–PD-1 mAb treatment of *Zeb1*^{iΔEC} mice resulted in a rapid tumor regression, and tumors began regressing by day 15 and eventually became undetectable by day 27 after tumor implantation (Figure 8, A and B). Furthermore, anti–PD-1 mAb treatment failed to increase survival in tumor-bearing *Zeb1*^{WT} mice, but markedly extended survival in tumor-bearing *Zeb1*^{iΔEC} mice (Figure 8C). All *Zeb1*^{iΔEC} mice treated with anti–PD-1 mAb survived through the observation period (200 days from tumor implantation), compared with none of the isotype control–treated *Zeb1*^{iΔEC} mice (median survival, 62 days), the isotype control–treated *Zeb1*^{WT} mice (median survival, 32 days), or the anti–PD-1–treated *Zeb1*^{WT} mice (median survival, 38 days) (Figure 8C). Finally, flow cytometry analyses revealed that treatment with anti–PD-1 mAb substantially increased infiltration of total, activated (CD69$^+$), and proliferative (Ki67$^+$) CD8$^+$ T cells and CD4$^+$ T cells in tumors of *Zeb1*^{iΔEC} mice compared with *Zeb1*^{WT} mice (Figure 8, D and E).

ZEB1 deletion epigenetically represses TGF-β signaling in tumor ECs. To characterize how ZEB1 deficiency regulates tumor EC phenotypes, we performed transcriptome RNA sequencing (RNA-Seq) in FACS-purified tumor ECs of *Zeb1*^{iΔEC} versus *Zeb1*^{WT} LLC tumors. Gene Ontology (GO) analysis demonstrated that ZEB1 deletion in tumor ECs downregulated the expression of signature genes enriched in TGF-β signaling and several other proangiogenic signaling pathways, such as mitogen-activated protein kinase (MAPK), Wnt, Ras, vascular endothelial growth factor (VEGF), Notch, and PI3K/Akt (Figure 9A). The TGF-β signaling pathway is thought to crosstalk and regulate these proangiogenic signaling pathways at multiple levels (38–41). Therefore, we reasoned that ZEB1 deficiency may regulate tumor EC phenotypes by

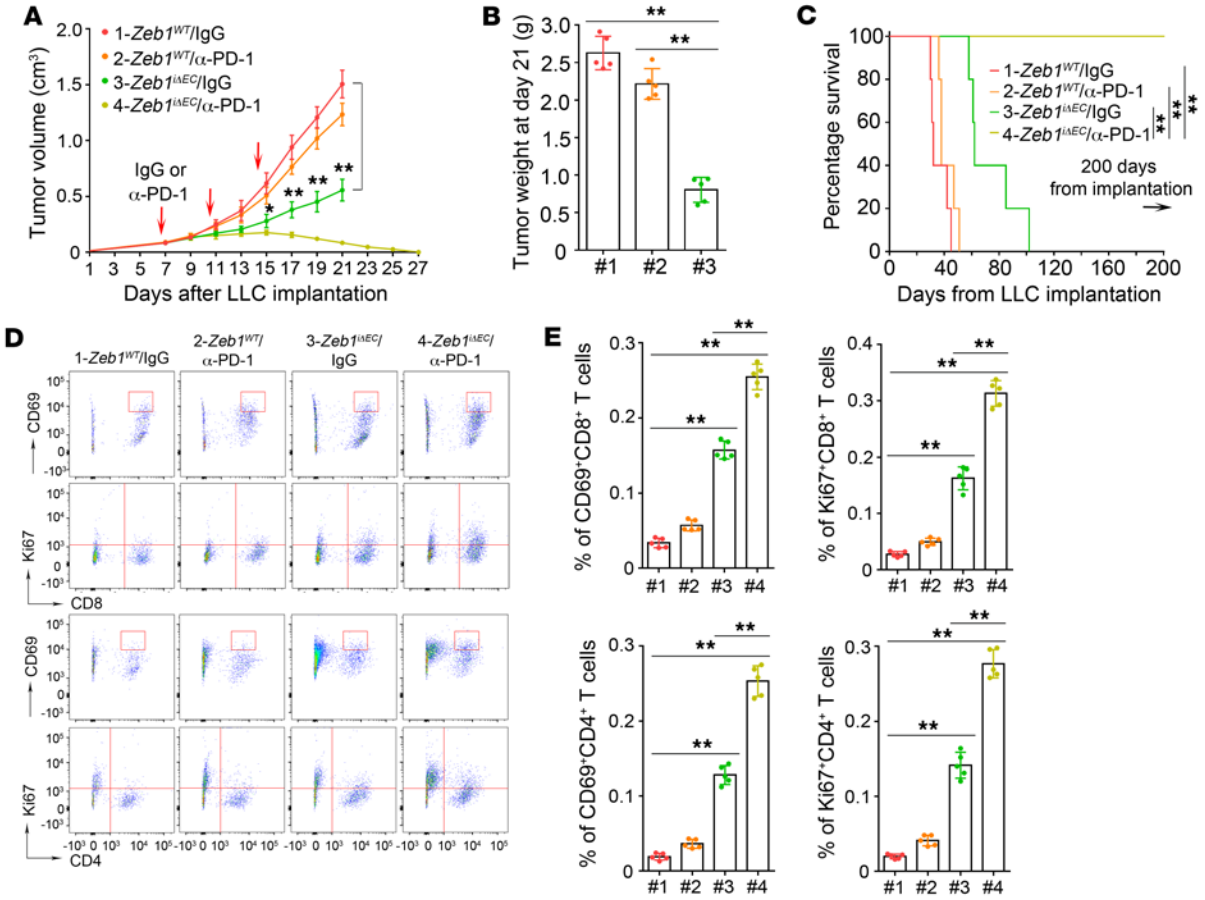

Figure 8. Endothelial ZEB1 deletion sensitizes LLC tumors to anti–PD-1 immunotherapy. (**A**) Growth curves of LLC tumors grown for 21 or 27 days in *Zeb1*^{WT} and *Zeb1*$^{i\Delta EC}$ mice that were treated with 200 μg isotope control (IgG) or anti–PD-1 mAb once every 3 days for a total of 3 times (5 mice each). (**B**) Comparison of tumor weight of the indicated LLC tumors harvested at day 21 after implantation (5 mice each). (**C**) Comparison of overall survival of the indicated LLC tumor–bearing mice as described in **A** (5 mice each). (**D** and **E**) Representative flow cytometric plots (**D**) and quantification (**E**) of CD69$^+$CD8$^+$, Ki67$^+$CD8$^+$, CD69$^+$CD4$^+$, and Ki67$^+$CD4$^+$ T cell fractions in LLC tumors of the indicated mice as described in **A** (5 mice each). Tumors were harvested for flow cytometric analysis at day 18 after implantation. All data are represented as mean ± SD. $^*P < 0.05$; $^{**}P < 0.01$. Differences were tested using 2-way ANOVA with Tukey's post hoc test (**A**), 1-way ANOVA with Tukey's post hoc test (**B** and **E**), and log-rank test (**C**).

repressing TGF-β signaling. Thus, we validated that FACS-purified *Zeb1*$^{i\Delta EC}$ tumor ECs displayed markedly reduced mRNA levels of TGF-β ligands including *Tgfb1*, *Tgfb2*, and *Tgfb3*, with no reduction in mRNA levels of the TGF-β receptors *Tgfbr1* and *Tgfbr2*, or the receptor-regulated SMADs (R-SMADs), including *Smad2* and *Smad3* (Figure 9B). In addition, immunofluorescence analysis revealed that TGF-β1 was abundantly expressed in LLC and B16F10 tumor ECs, and vascular TGF-β1 expression was remarkably decreased in LLC and B16F10 tumors grown in *Zeb1*$^{i\Delta EC}$ mice compared with *Zeb1*^{WT} mice (Figure 9, C and D, and Supplemental Figure 7, A and B). Consistently, the analyses revealed markedly diminished distribution of p-SMAD2/3, an active form of R-SMADs that can translocate into the nucleus to initiate transcription of TGF-β–targeting genes, along blood vessels of LLC and B16F10 tumors grown in *Zeb1*$^{i\Delta EC}$ mice compared with *Zeb1*^{WT} mice. Also, p-SMAD2/3 levels in vessel-excluded areas at LLC and B16F10 tumors of *Zeb1*$^{i\Delta EC}$ mice were reduced in comparison with *Zeb1*^{WT} mice (Figure 9, E and F, and Supplemental Figure 7, C and D). Given that TGF-βs function as autocrine or paracrine signaling molecules within the TME, we assessed the impact of vascular ZEB1 deletion on the secretion of TGF-βs in LLC tumors. Indeed, ELISA of LLC whole tumor lysates revealed that the levels of secreted TGF-β1, TGF-β2, and TGF-β3 were significantly decreased in tumors of *Zeb1*$^{i\Delta EC}$ mice relative to *Zeb1*^{WT} mice (Figure 9G). These findings suggest that vascular ZEB1 deletion reduces expression and secretion of these 3 TGF-β isoforms to the TME, which diminishes tumor vascular TGF-β receptor signaling in an autocrine fashion while reducing TGF-β receptor signaling in non-ECs in a paracrine fashion.

We next questioned whether endothelial ZEB1 deletion downregulates TGF-β signaling in a tumor EC–autonomous fashion. To this end, LLC tumor ECs of *Zeb1*$^{fl/fl}$ mice were purified and infected with adeno–β-gal and adeno-Cre to generate control and ZEB1-deleted LLC tumor ECs, and infected cells were subjected to multiple analyses. As shown, *Zeb1*, *Tgfb1*, *Tgfb2*, and *Tgfb3* transcript levels were significantly reduced in ZEB1-deleted tumor ECs compared with control cells (Figure 10A). Also, ZEB1 deletion in tumor ECs decreased ZEB1, TGF-β1, and p-SMAD2/3 protein levels without affecting total SMAD2/3 expression, as assessed by immunoblot analysis (Figure 10B and Supplemental Figure 7E).

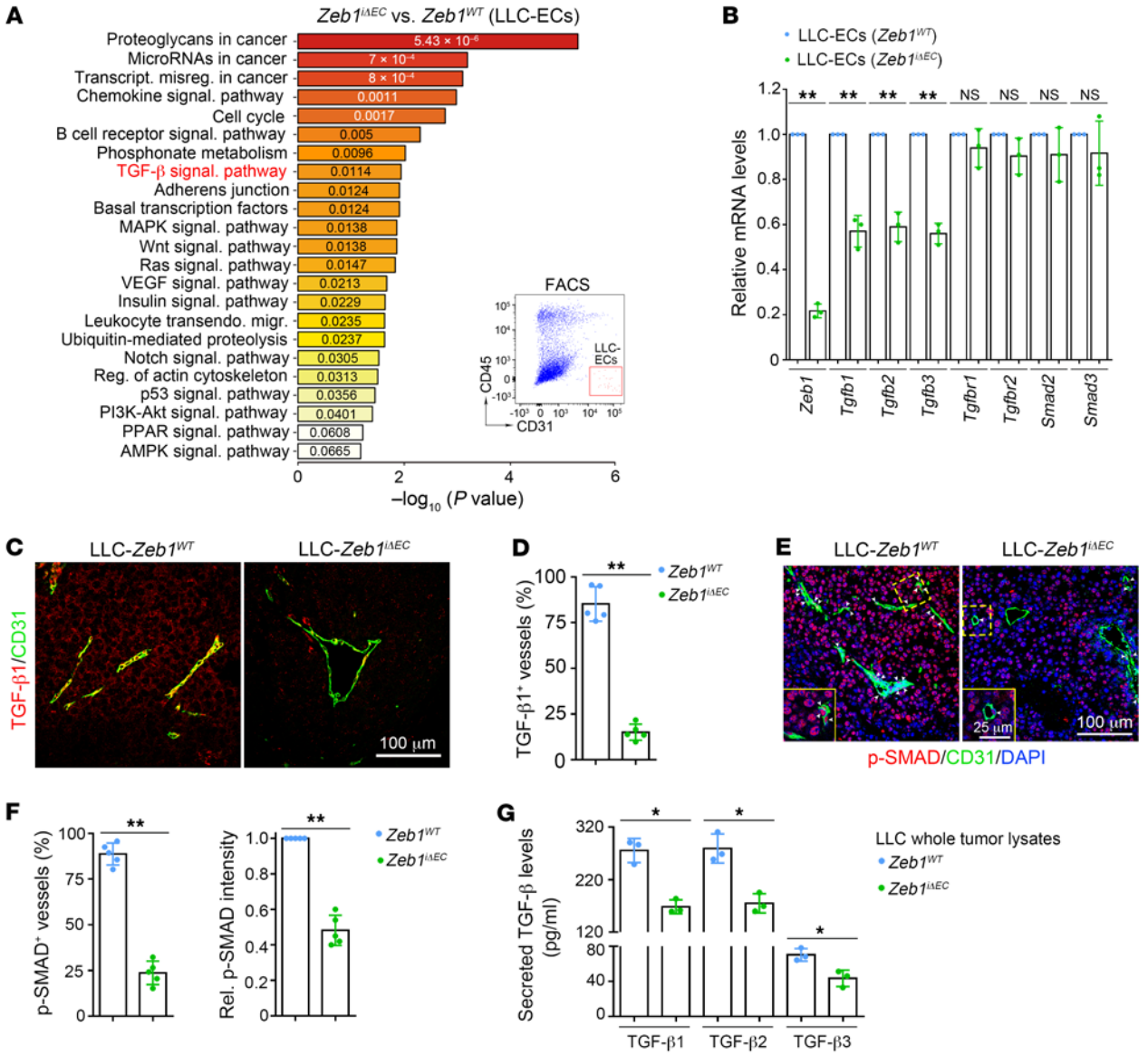

Figure 9. Vascular ZEB1 inactivation represses TGF-β expression and secretion in the LLC tumor. (**A**) GO analysis of signature genes that are differentially expressed in FACS-isolated ECs dissected from LLC tumors of *Zeb1*^{WT} and *Zeb1*$^{i\Delta EC}$ mice, revealing significantly modulated functional pathways. (**B**) qRT-PCR analyses of indicated gene expression in FACS-isolated ECs dissected from LLC tumors of *Zeb1*^{WT} and *Zeb1*$^{i\Delta EC}$ mice (n = 3 independent experiments). (**C** and **D**) Immunofluorescent images (**C**) and comparison (**D**) of TGF-β1$^+$ BVs in LLC tumors of *Zeb1*^{WT} versus *Zeb1*$^{i\Delta EC}$ mice (5 mice each). (**E** and **F**) Immunofluorescent images (**E**) and comparison (**F**) of p-SMAD2/3$^+$ BVs in LLC tumors of *Zeb1*^{WT} versus *Zeb1*$^{i\Delta EC}$ mice (5 mice each). Comparison of p-SMAD2/3 expression in vessel-excluded areas at the indicated tumors is shown in **F** (right). (**G**) ELISA for secreted TGF-β1, TGF-β2, and TGF-β3 levels in whole lysates of LLC tumors dissected from *Zeb1*^{WT} and *Zeb1*$^{i\Delta EC}$ mice (n = 3 independent experiments). All data are represented as mean ± SD. *P < 0.05; **P < 0.01. Differences were tested using unpaired 2-sided Student's t test.

Furthermore, a promoter luciferase reporter assay showed that transcription of *Tgfb1*, *Tgfb2*, and *Tgfb3* was markedly reduced in ZEB1-deleted tumor ECs compared with control cells (Figure 10C). Using chromatin immunoprecipitation (ChIP) assays, we confirmed the loading of ZEB1 onto the proximal but not the distal regions of *Tgfb1*, *Tgfb2*, and *Tgfb3* promoters in LLC tumor ECs (Figure 10D). ZEB1 is primarily known as a transcriptional repressor that induces EMT by suppressing *CDH1* transcription (19–22). However, our findings suggest that ZEB1 can be a transcriptional activator that enhances transcription of *Tgfb* in tumor ECs. Next, we investigated how ZEB1 deletion reduces *Tgfb1*, *Tgfb2*, and *Tgfb3* transcript levels in tumor ECs. Transcription factors are known to transactivate target genes by recruiting coactivators to promoters of target genes, which can increase histone acetylation on the promoters and thus induces transcriptional activation (42, 43). ChIP analyses were performed in control and ZEB1-deleted tumor ECs, and the results showed that ZEB1 deletion in tumor ECs markedly reduced histone acetylation, including histone H3 lysine 4 acetylation (H3K4Ac), H3K14Ac, and H3K18Ac, on the promoters of *Tgfb1*, *Tgfb2*, and *Tgfb3*, without affecting levels of histone H3 lysine 27 trimethylation (H3K27me3), a reported repressive histone marker, at the promoters (42, 44) (Figure 10E and Sup-

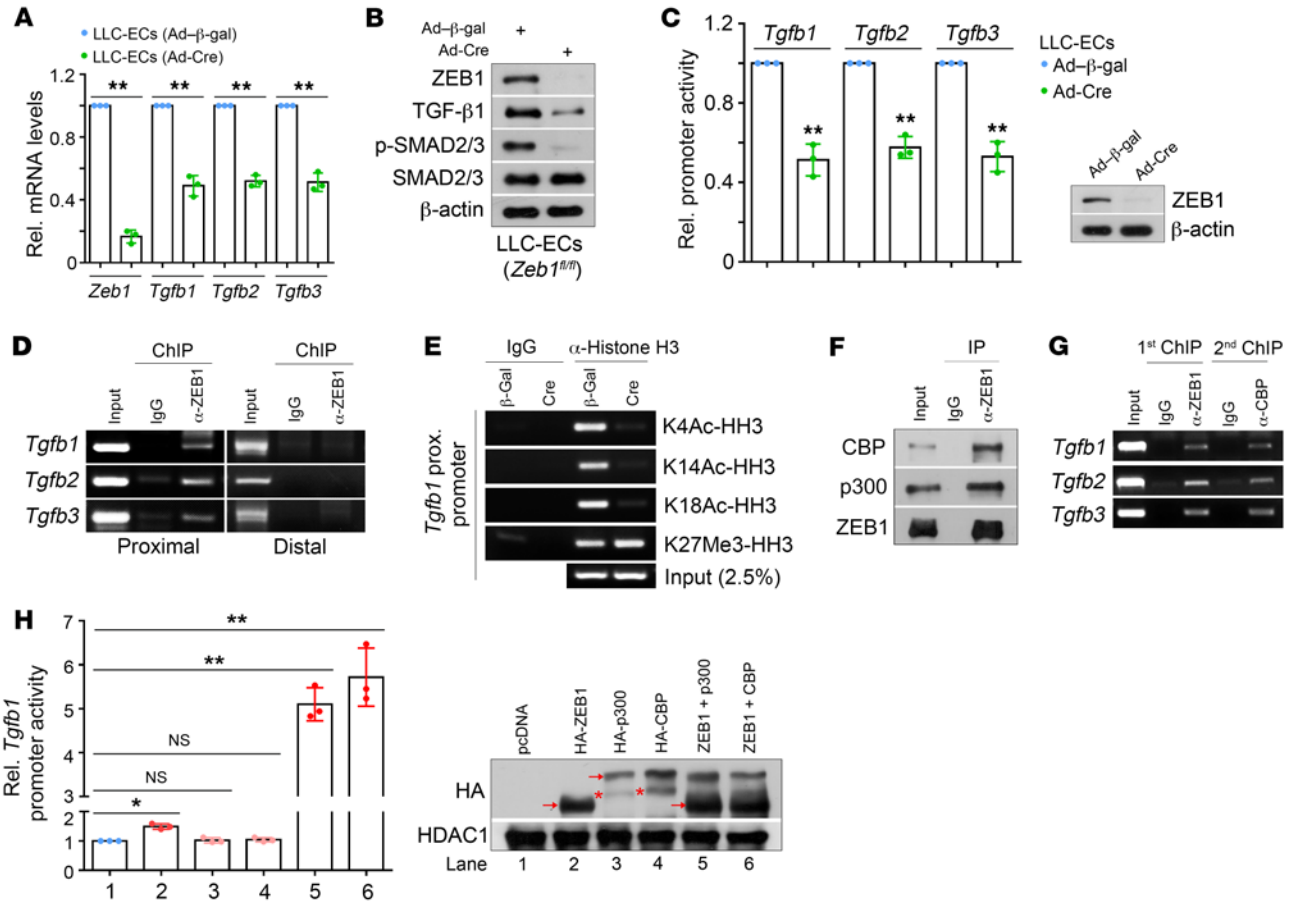

Figure 10. ZEB1 deletion epigenetically represses TGF-β signaling in LLC tumor ECs. (**A**) Comparison of indicated gene expression in the in vitro–cultured control (i.e., Ad–β-gal–infected) versus ZEB1-deleted (i.e., Ad-Cre–infected) LLC tumor ECs (n = 3 independent experiments). (**B**) Immunoblot analysis of control and ZEB1-deleted tumor ECs as described in **A**. (**C**) Luciferase reporter analysis of control and ZEB1-deleted LLC-ECs that were transfected with *Tgfb1*, *Tgfb2*, and *Tgfb3* promoter reporter constructs (n = 3 independent experiments). Right panel: immunoblot analysis of ZEB1 expression in control and ZEB1-deleted LLC-ECs. (**D**) ChIP-PCR for confirming the loading of ZEB1 on the proximal but not distal promoters of *Tgfb1*, *Tgfb2*, and *Tgfb3* in LLC-ECs (n = 3 independent experiments). Around 5 × 10^6 LLC-ECs were used for each ChIP-PCR experiment. (**E**) ChIP-PCR for analyzing the enrichments of H3K4Ac, H3K14Ac, H3K18Ac, and H3K27me3 on *Tgfb1* promoter in control and ZEB1-deleted LLC-ECs (n = 3 independent experiments). (**F**) IP analysis confirming association of endogenous ZEB1 with CBP or p300 in LLC-ECs (n = 3 independent experiments). (**G**) Sequential ChIP-PCR for analyzing the co-occupancy of ZEB1 and CBP on the promoters of *Tgfb1*, *Tgfb2*, and *Tgfb3* (n = 3 independent experiments). (**H**) Luciferase reporter assays for analyzing *Tgfb1* promoter activity in HEK293T cells that were cotransfected with the indicated constructs (n = 3 independent experiments). Right panel: immunoblot analysis confirming ectopic expression of HA-tagged ZEB1, p300, and CBP in HEK293T cells. Asterisks and arrows mark nonspecific bands and specific bands, respectively, with the expected molecular weights. All data are represented as mean ± SD. *P < 0.05; **P < 0.01. Differences were tested using unpaired 2-sided Student's t test (**A** and **C**) and 1-way ANOVA with Tukey's post hoc test (**H**).

plemental Figure 7F). To uncover the coactivators responsible for histone acetylation on the promoters of *Tgfb* genes, we performed coimmunoprecipitation experiments in LLC tumor ECs. Indeed, we found that ZEB1 was physically associated with the histone acetyltransferases CREB-binding protein (CBP) and p300 in tumor ECs (Figure 10F). Sequential ChIP analyses revealed that ZEB1 and CBP co-occupied the promoters of *Tgfb1*, *Tgfb2*, and *Tgfb3* in tumor ECs (Figure 10G). Finally, a promoter luciferase reporter assay was performed in 293T cells that were transiently transfected with HA-ZEB1, HA-p300, or HA-CBP alone, or ZEB1 in combination with p300 or CBP (Figure 10H). The results demonstrated that overexpression of ZEB1, p300, or CBP alone increased *Tgfb1* promoter activity by 50%, 1%, or 2%, respectively, while overexpression of ZEB1 in combination with p300 or CBP resulted in a 5.1-fold or 5.7-fold increase in *Tgfb1* promoter activity, respectively (Figure 10H). These findings suggest that CBP/p300 interacts with ZEB1 and they co-occupy the promoters of *Tgfb* genes to induce transcriptional activation in tumor ECs.

Administration of recombinant Tgfb1 protein to Zeb1$^{i\Delta EC}$ mice disrupts tumor vascular normalization and recovers the impaired cancer growth and progression. We next evaluated whether ZEB1 deletion in cultured LLC tumor ECs can also reduce the secretion of TGF-βs. To this end, conditioned medium (CM) of control and ZEB1-deleted tumor ECs (designated control CM and ZEB1-deleted CM, respectively) was collected, and ELISAs were performed. The results showed that secreted TGF-β1, TGF-β2, and TGF-β3 levels were remarkably reduced in ZEB1-deleted CM compared with control CM (Supplemental Figure 8A). Consistent with these findings, LLC tumor cells in the presence of ZEB1-deleted CM or control non-CM exhibited substantially decreased p-SMAD2/3

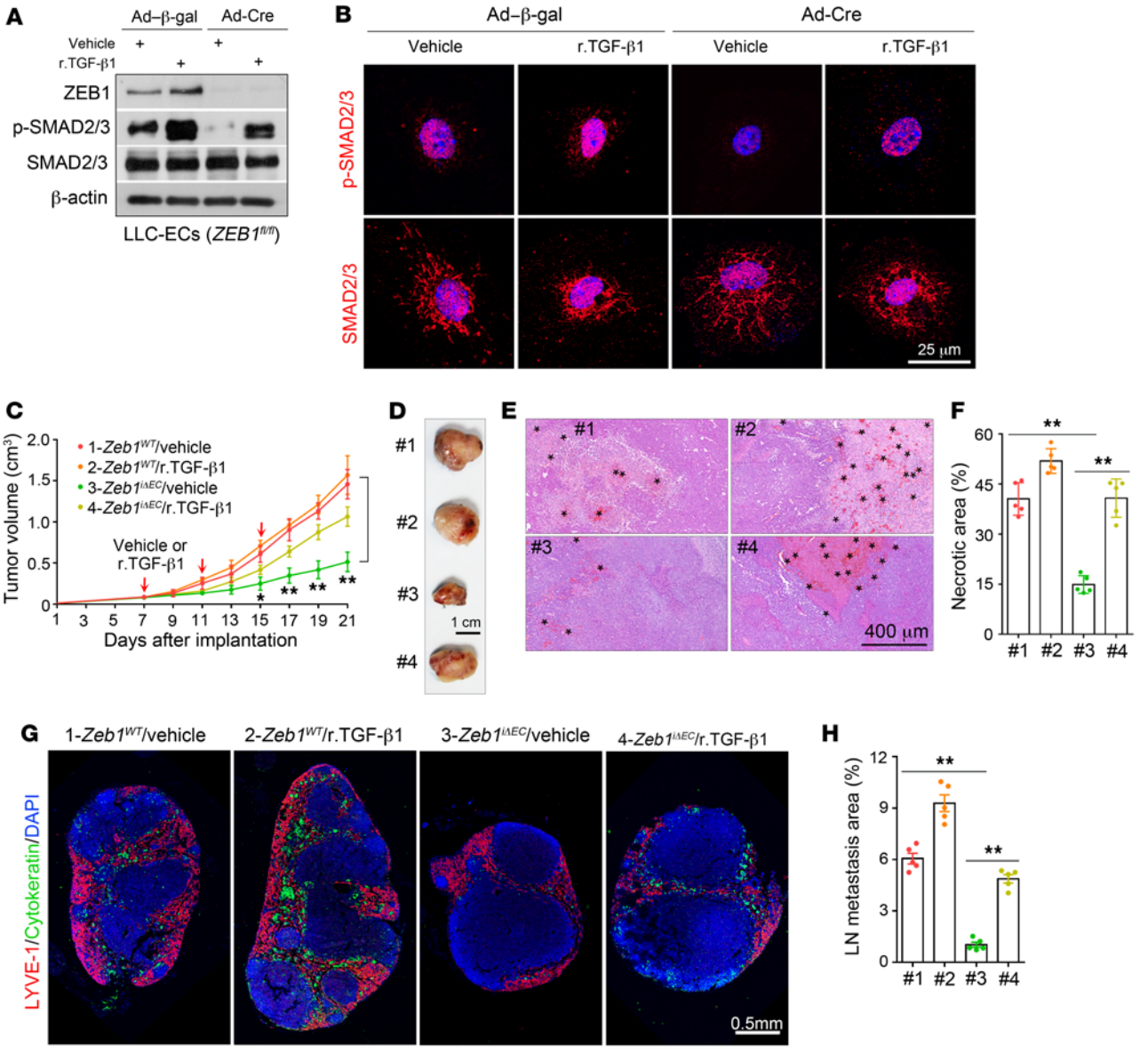

Figure 11. Treatment of *Zeb1*$^{i\Delta EC}$ mice with r.TGF-β1 protein recovers impaired tumor progression. (**A**) Immunoblot analysis of control (i.e., Ad–β-gal–infected) and ZEB1-deleted (i.e., Ad-Cre–infected) LLC tumor ECs that were treated with vehicle or 2 ng/mL r.TGF-β1 protein for 3 hours. (**B**) Immunofluorescent images showing p-SMAD2/3 (top) and SMAD2/3 (bottom) expression in the indicated cells as described in **A**. Nuclei, DAPI (blue). (**C**) Growth curves of LLC tumors grown for 21 days in *Zeb1*^{WT} and *Zeb1*$^{i\Delta EC}$ mice that were treated with vehicle or 1.3 μg/kg r.TGF-β1 protein once every 3 days for a total of 3 times (5 mice each). (**D**) Gross images of freshly dissected tumors as described in **C**. (**E** and **F**) H&E-stained images (**E**) and quantification (**F**) of hemorrhagic necrosis in LLC tumors of vehicle- or r.TGF-β1–treated *Zeb1*^{WT} and *Zeb1*$^{i\Delta EC}$ mice as described in **C** (5 mice each). Asterisks in **E** denote hemorrhagic foci. (**G** and **H**) Immunofluorescent images (**G**) and comparison (**H**) of metastasized cytokeratin$^+$ LLC tumor cells in the inguinal LNs of tumor-bearing mice as described in **C** (5 mice each). The cytokeratin$^+$ area is presented as a percentage of sectional area. All data are represented as mean ± SD. $^*P < 0.05$; $^{**}P < 0.01$. Differences were tested using 2-way ANOVA with Tukey's post hoc test (**C**) and 1-way ANOVA with Tukey's post hoc test (**F** and **H**).

levels relative to tumor cells in control CM (Supplemental Figure 8B). Notably, ZEB1 protein was undetectable in LLC tumor cells in the presence of control non-CM, control CM, or ZEB1-deleted CM (Supplemental Figure 8B). Next, we set up to determine whether ZEB1 deletion in tumor ECs can affect LLC tumor cell proliferation in a paracrine fashion. To this end, tumor cells were cultured in control non-CM supplemented with 10% FBS and then in control non-CM, control CM, or ZEB1-deleted CM supplemented with 0.5% FBS, and cell numbers were counted. As shown, LLC tumor cells grew at a comparable rate in the presence of control non-CM, control CM, or ZEB1-deleted CM within 36 hours of culture, while tumor cells in the presence of control CM proliferated at a significantly higher rate than cells in control non-CM or ZEB1-deleted CM at 60 and 84 hours of culture (Supplemental Figure 8C). Moreover, we assessed the impact of tumor vascular ZEB1 deletion on LLC tumor cell invasion. To this end, tumor cells were cultured in medium without FBS in the upper chambers of Transwell inserts with an 8-μm pore size that were precoated

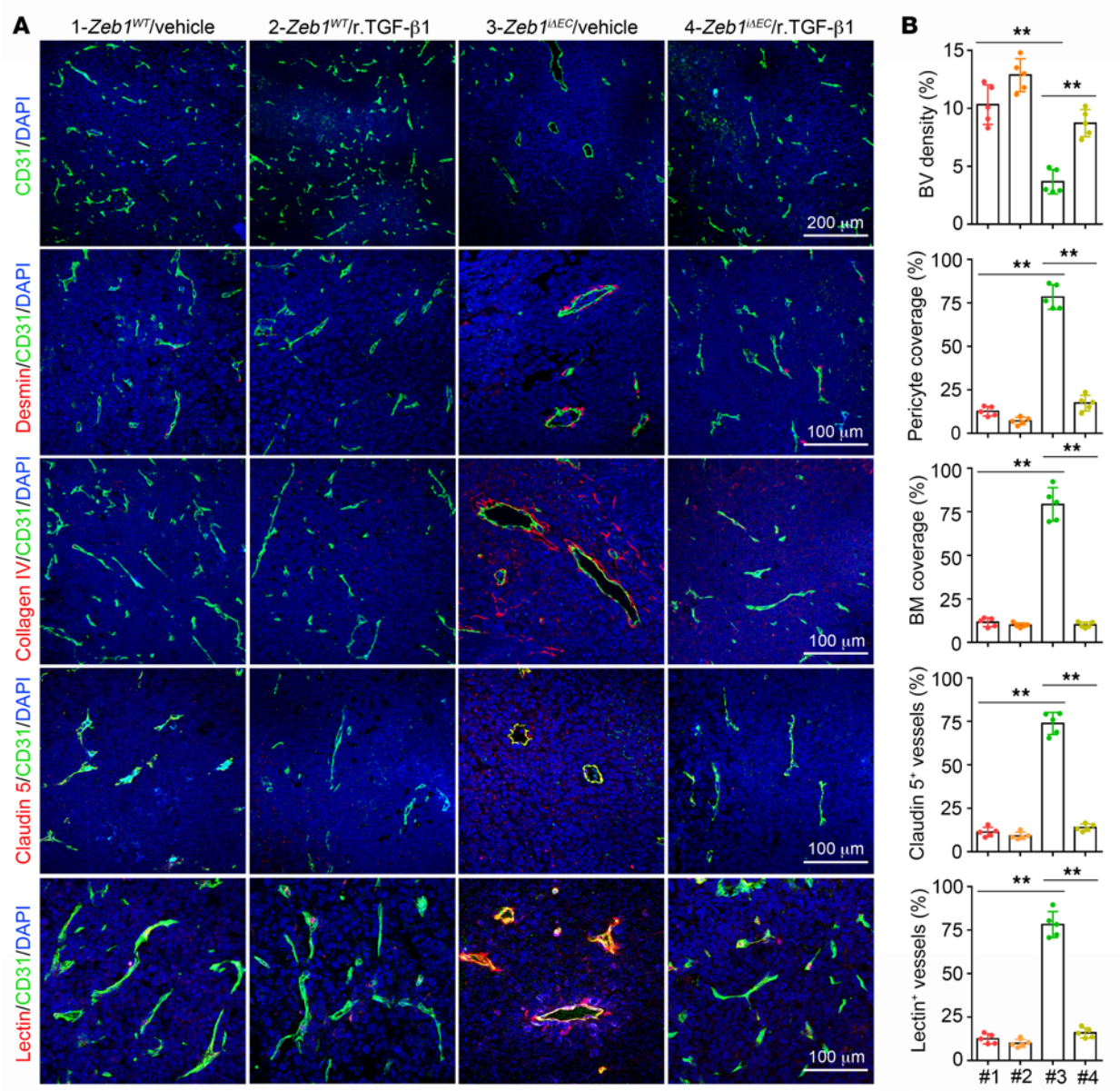

Figure 12. Treatment with r.TGF-β1 protein disrupts tumor vessel normalization and perfusion in *Zeb1*$^{i\Delta EC}$ mice. (**A** and **B**) Immunofluorescent images (**A**) and comparisons (**B**) of BV density, desmin$^+$ pericyte and collagen type IV$^+$ BM coverages along BVs, claudin 5 distribution on BVs, and lectin perfusion of BVs in LLC tumors dissected from the indicated mice (5 mice each). All data are represented as mean ± SD. $^{**}P < 0.01$. Differences were tested using 1-way ANOVA with Tukey's post hoc test.

with Matrigel, while the lower chambers were filled with control non-CM, control CM, or ZEB1-deleted CM. Indeed, we found a marked reduction in numbers of invaded tumor cells in the presence of ZEB1-deleted CM or control non-CM compared with control CM (Supplemental Figure 8, D and E). Altogether, these results suggest that endothelial ZEB1 deletion strongly reduces tumor cell growth and invasion by diminishing TGF-β/SMAD signaling in tumor cells (in a paracrine fashion).

Given these results, we set up to assess the degree to which tumor vasculature–derived TGF-βs serve as ZEB1 target substrates required for cancer growth and progression. As shown, in vitro treatment with recombinant TGF-β1 (r.TGF-β1) protein fully restored SMAD activity in ZEB1-deleted LLC tumor ECs (Figure 11, A and B), suggesting that ZEB1-deleted ECs can respond to TGF-β1 stimulation. We next determined whether in vivo administration of r.TGF-β1 protein can restore impaired cancer growth and metastasis. To this end, vehicle or r.TGF-β1 protein (1.3 μg/kg body weight) was intravenously injected into *Zeb1*$^{i\Delta EC}$ and *Zeb1*^{WT} mice every 3 days for a total 3 times starting when tumor volume reached 100 mm^3 (6–7 days after LLC tumor implantation). Treatment with r.TGF-β1 had no obvious impact on LLC tumor growth in *Zeb1*^{WT} mice, but significantly restored the impaired tumor growth in *Zeb1*$^{i\Delta EC}$ mice (Figure 11, C and D). Consistently, reduced intratumoral necrosis with hemorrhagic foci and shrunk hypoxic area (as evidenced by decreased expression levels of pimonidazole and GLUT1) were efficiently restored in LLC tumors of r.TGF-β1–treated *Zeb1*$^{i\Delta EC}$ mice compared with vehicle-treated *Zeb1*$^{i\Delta EC}$ mice (Figure 11, E and F, and

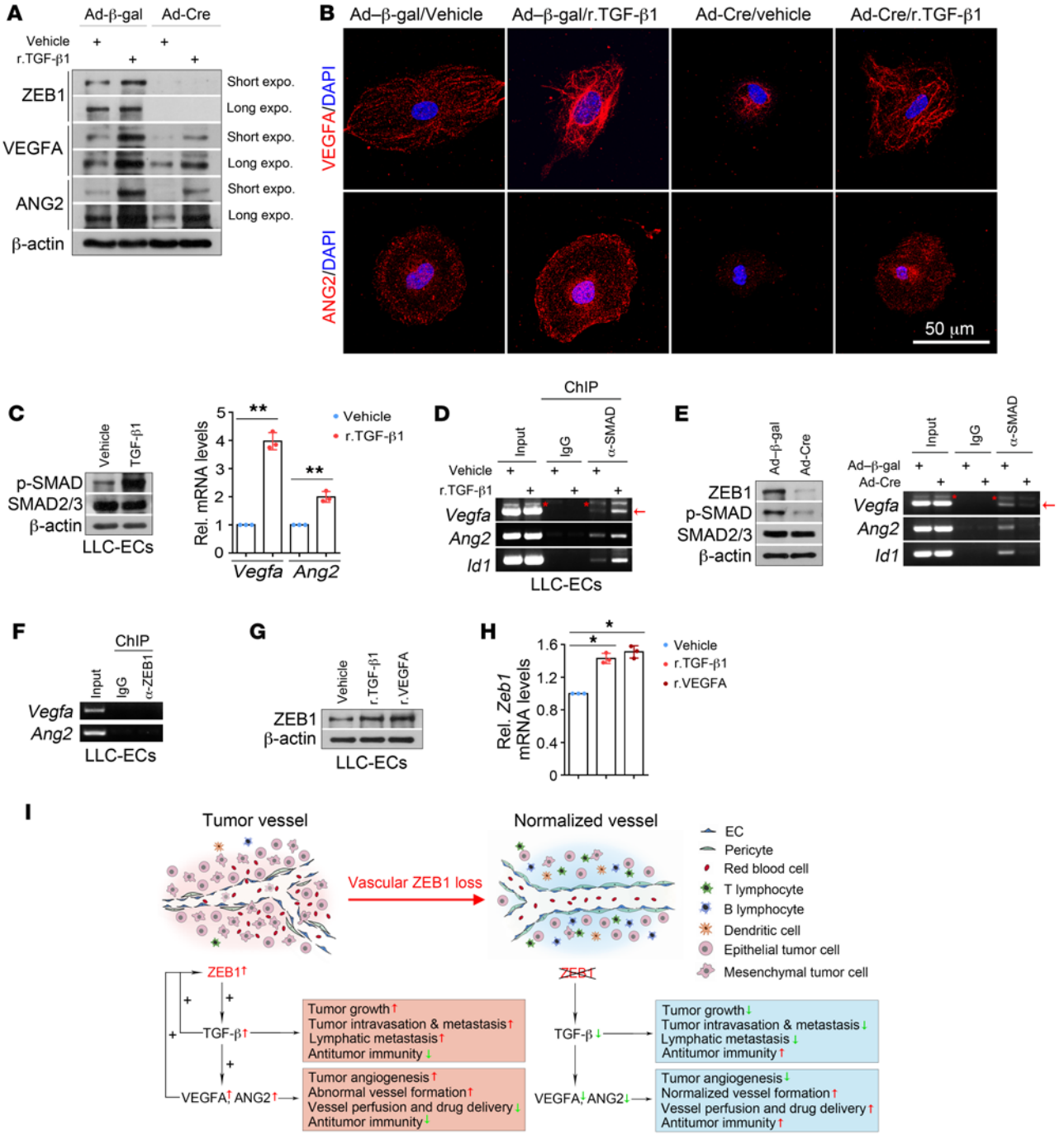

Figure 13. ZEB1/TGF-β/SMAD signaling transactivates *Vegfa* and *Ang2* genes in LLC tumor ECs. (**A**) Immunoblot analysis of control and ZEB1-deleted LLC-ECs that were treated with vehicle or 2 ng/mL r.TGF-β1 protein for 3 hours. (**B**) Immunofluorescence analysis of VEGFA (top) and ANG2 (bottom) expression in the indicated cells as described in **A**. Nuclei, DAPI (blue). (**C**) Immunoblot (left) and qRT-PCR (right) analyses of vehicle- or r.TGF-β1–treated LLC-ECs for p-SMAD2/3 and SMAD2/3 protein expression and *Vegfa* and *Ang2* mRNA expression (n = 3 independent experiments). (**D**) ChIP-PCR for assessing SMAD2/3 level on the promoters of *Vegfa*, *Ang2*, and *Id1* in vehicle- and r.TGF-β1–treated LLC-ECs (n = 3 independent experiments). Around 5×10^6 LLC-ECs were used for each ChIP-PCR experiment. (**E**) ChIP-PCR for assessing SMAD2/3 level on the promoters of *Vegfa*, *Ang2*, and *Id1* in control and ZEB1-deleted LLC-ECs (n = 3 independent experiments). Left panel: immunoblot analysis for confirming reduced ZEB1 and p-SMAD2/3 expression in ZEB1-deleted LLC-ECs. (**F**) ChIP-PCR showing no binding of ZEB1 on the proximal promoters of *Vegfa* and *Ang2* in LLC-ECs (n = 3 independent experiments). (**G** and **H**) Immunoblotting (**G**) and qRT-PCR (**H**) for assessing ZEB1 protein and mRNA expression in LLC-ECs treated with vehicle, r.TGF-β1 (2 ng/mL, 3 hours), or r.VEGFA (20 ng/mL, 18 hours) (n = 3 independent experiments). (**I**) Schematic diagram showing the effect of vascular ZEB1 loss on tumor growth and metastasis, tumor angiogenesis, vascular functionality and integrity, and tumor immune microenvironment. All data are represented as mean ± SD. $^*P < 0.05$; $^{**}P < 0.01$. Differences were tested using unpaired 2-sided Student's t test (**C**) and 1-way ANOVA with Tukey's post hoc test (**H**).

Supplemental Figure 8, F and G). Also, the abilities of LLC tumor cells to metastasize to inguinal LNs were markedly recovered in r.TGF-β1–treated tumor-bearing *Zeb1*$^{i\Delta EC}$ mice (Figure 11, G and H). Moreover, diminished tumor vascular densities were substantially reversed in tumors of r.TGF-β1–treated *Zeb1*$^{i\Delta EC}$ mice (Figure 12, A and B). Notably, administration of r.TGF-β1 protein to LLC tumor–bearing *Zeb1*$^{i\Delta EC}$ mice considerably disrupted tumor vessel normalization, as evidenced by diminished desmin$^+$ pericyte coverage on tumor vessels, reduced collagen type IV$^+$ BM coverage along blood vessels, impaired claudin 5 distribution on tumor vessels, and impeded tumor vessel perfusion (measured by a labeled-lectin perfusion assay) (Figure 12, A and B). Collectively, these findings suggest that the ZEB1/TGF-β axis in the TME plays an important role in tumor growth and metastasis.

We next determined whether forced expression of TGF-β1 in tumor cells could counteract the effect of targeting endothelial ZEB1. To this end, LLC tumor cells were infected with pLenti-lox or pLenti-lox-TGF-β1-HA lentiviral vectors (to generate LLC-control or LLC–TGF-β1 tumor cells; Supplemental Figure 9, A and B) and subcutaneously injected into *Zeb1*^{WT} and *Zeb1*$^{i\Delta EC}$ mice, respectively, and tumor growth, vascular functional integrity, and tumor angiogenesis were evaluated. As shown, while LLC–TGF-β1 tumors and LLC-control tumors grew at largely comparable rates in *Zeb1*^{WT} mice, LLC–TGF-β1 tumor growth was greatly promoted in *Zeb1*$^{i\Delta EC}$ mice compared with LLC-control tumors of *Zeb1*$^{i\Delta EC}$ mice (Supplemental Figure 9C), phenocopying the administration of r.TGF-β1 protein to LLC tumor–bearing *Zeb1*^{WT} and *Zeb1*$^{i\Delta EC}$ mice. Compared with LLC-control tumors grown in *Zeb1*$^{i\Delta EC}$ mice, LLC–TGF-β1 tumors of *Zeb1*$^{i\Delta EC}$ mice exhibited enhanced tumor vessel density, impaired desmin$^+$ pericyte and collagen IV$^+$ BM coverages along tumor vessels, and diminished claudin 5$^+$ distribution on tumor vessels (Supplemental Figure 9, D and E). These findings suggest that forced expression of TGF-β1 in tumor cells markedly counteracts the effect of targeting endothelial ZEB1 in mice.

ZEB1/TGF-β/SMAD signaling transactivates VEGFA and ANG2 genes in tumor ECs. Given that TGF-β is not directly angiogenic, we speculated that the signaling molecules that are directly angiogenic might mediate the effect of ZEB1/TGF-β signaling on the regulation of tumor angiogenesis and vessel functionality and integrity. To test this, *Zeb1*$^{fl/fl}$ LLC tumor ECs were infected with adeno–β-gal or adeno-Cre to generate control and ZEB1-deleted cells, treated with vehicle or 2 ng/mL r.TGF-β1 protein for 3 hours, and subjected to immunoblot and immunofluorescence analyses. As shown, treatment of control or ZEB1-deleted tumor ECs with TGF-β1 markedly increased protein levels of VEGF and angiopoietin-2 (ANG2), two potent proangiogenic cytokines that sustain tumor angiogenesis directly (37, 45, 46) (Figure 13, A and B); VEGFA and ANG2 protein levels were remarkably diminished in ZEB1-deleted LLC tumor ECs compared with control cells (Figure 13, A and B). Also, qRT-PCR analysis revealed that *Vegfa* and *Ang2* transcript levels were profoundly increased in TGF-β1–treated tumor ECs compared with vehicle-treated cells (Figure 13C). Further, we performed SMAD2/3 ChIP assays and found that SMAD indeed bound to the promoters of *Id1* (a classic TGF-β/SMAD target gene), *Vegfa*, and *Ang2*, and the levels of SMAD binding on the *Id1*, *Vegfa*, and *Ang2* promoters were robustly increased following TGF-β1 treatment (Figure 13D). Conversely, ZEB1 deletion reduced TGF-β activity, which consequently diminished SMAD on the promoters of *Id1*, *Vegfa*, and *Ang2* (Figure 13E). These results suggest that, like *Id1*, *Vegfa* and *Ang2* are direct target genes of TGF-β/SMAD signaling in tumor ECs. To determine whether ZEB1 directly targets the promoters of *Vegfa* and *Ang2*, we performed ZEB1 ChIP assays and found that ZEB1 was not recruited to *Vegfa* and *Ang2* promoters (Figure 13F). Importantly, we observed that r.TGF-β1 and r.VEGFA upregulated ZEB1 expression at both the protein and the mRNA level in LLC tumor ECs (Figure 13, G and H), creating positive-feedback loops that potentiate ZEB1-stimulated TGF-β1 and VEGFA expression.

Discussion

ZEB1 has been extensively studied in cancer cells and is known to function as an important driver of cancer invasion, metastasis, and treatment resistance by inducing the so-called epithelial-mesenchymal transition (EMT) in cancer cells (19, 20, 22, 23). However, immunohistochemical staining of clinical tumor samples of various cancer types reveals predominant expression of ZEB1 in the tumor stromal compartment with low expression or loss of expression of ZEB1 in the tumor epithelial compartment (24–27). Here we confirm that ZEB1 is not expressed in the tested murine cancer cell lines in culture or upon tumor formation in vivo, but highly expressed in CD31$^+$ tumor vessels of ectopic and orthotopic tumors. We further discover that ZEB1 expression is largely confined to tumor vascular ECs, only occasionally present in other cells in tumor stroma, and absent in leukocytes. Notably, we find low expression or loss of expression of ZEB1 in normal tissues. In line with this significantly distinct expression pattern of ZEB1 in normal tissue versus tumor tissue, deletion of vascular ZEB1 in adult mice does not induce growth retardation, differences in vascular morphology and density, or histological alterations in major organs, while vascular ZEB1 deficiency in tumor-bearing mice results in impaired tumor growth, intravasation, and metastasis. Most importantly, we uncover that vascular ZEB1 expression levels in human lung adenocarcinomas are significantly higher than those in matched adjacent lung tissue, and correlate negatively with survival rates in lung cancer patients. These data suggest, for what we believe is the first time, that high expression of vascular ZEB1 in lung cancer or other cancer types is a negative prognostic factor in these patients, further highlighting ZEB1 as a clinically relevant therapeutic target in advanced cancer.

In the present study, we discover that vascular ZEB1 inactivation suppresses the formation of tumor vessels and induces persistent normalization of remaining tumor vessels, thus diminishing cancer progression in multiple tumor models. Typical phenotypes of normalized tumor vessels are present in endothelial ZEB1–deleted tumors, including enhanced pericyte and BM coverage, improved tumor vessel perfusion, and reduced vascular permeability. Tumor vascular normalization is known to elicit enhanced tumor oxygenation, reduced hemorrhagic necrosis, and decreased interstitial pressure in the tumor, which consequently enhances delivery and efficacy of anticancer drugs (5, 6, 29, 47). This provides a rationale for the combination therapy of ZEB1 blockade and the conventional chemotherapeutic agent cisplatin. As a DNA damage–inducing drug, cisplatin may induce severe systematic side effects when used alone or in combination

with other drugs, which markedly limits its clinical implication. Here we find that low-dose cisplatin (one-fifth to one-tenth of a regular dose) has a significantly inhibitory effect on the growth of *Zeb1*$^{i\Delta EC}$ tumors with well-perfused vessels but does not elicit any obvious adverse effects in the mice, implying therapeutic potential of targeting ZEB1. As we believe that, like genetic inactivation of ZEB1, pharmacological targeting of ZEB1 may also exert potent anticancer therapeutic effects without affecting vasculatures or eliciting histological alterations in major organs, we are in the early stages of expressing and purifying human ZEB1 protein and ZEB1 fragmental proteins (i.e., N-, middle-, and C-terminus) for crystal structure analysis. Small-molecule ZEB1 inhibitors will be screened on the basis of ZEB1 crystal structures, and anticancer therapeutic effects of ZEB1 small-molecule inhibitors used in combination with low-dose conventional chemotherapy agents or immune checkpoint–blocking antibodies will be evaluated.

ZEB1 is primarily known as a transcriptional repressor that induces EMT programs in cancer cells by suppressing adherent proteins such as E-cadherin (19, 20, 22). Accumulating evidence suggests that ZEB1 could also be a transcriptional activator (21, 48, 49); however, the mechanism and significance of ZEB1 as an activator remain largely elusive. Here we provide evidence demonstrating that endothelium-derived ZEB1 functions as a transcriptional activator of *Tgfb1*, *Tgfb2*, and *Tgfb3* genes (genes that encode 3 TGF-β isoforms) by increasing histone acetylation on their promoters. We further demonstrate that, like *Id1*, a classic TGF-β direct target gene, *Vegfa* and *Ang2* are both direct target genes of TGF-β/SMAD signaling in tumor ECs. ZEB1 itself does not directly target *Vegfa* and *Ang2* promoters. Given that VEGFA and ANG2 are both directly angiogenic, we propose that these 2 potent proangiogenic cytokines mediate the effect of vascular ZEB1/TGF-β signaling on the regulation of tumor angiogenesis, vascular functionality and integrity, tumor vessel perfusion, and drug delivery (Figure 13I). Notably, the regulation mediated by the ZEB1/TGF-β/VEGFA-ANG2 signaling axis is of self-reinforcement (Figure 13I), further supporting the notion that the transcription activator ZEB1 has a key functional role in tumor endothelium. ELISA of whole tumor lysates derived from *Zeb1*^{WT} and *Zeb1*$^{i\Delta EC}$ mice reveals that targeting vascular ZEB1 results in a 40% reduction in secretion of each TGF-β isoform (TGF-β1, TGF-β2, and TGF-β3) to the TME, due to profoundly higher expression of ZEB1 in tumor ECs than in non-ECs. Accordingly, TGF-β receptor signaling (as shown by p-SMAD expression) in vessel-excluded areas at the *Zeb1*$^{i\Delta EC}$ tumors is reduced by 52%, an inhibition efficiency comparable to that of anti–TGF-β antibody treatment (50). In considering that these 3 TGF-β isoforms are all known to promote tumor growth, EMT-associated intravasation and metastasis, and tumor-induced immune suppression (Figure 13I) (35, 39, 40, 50–53), we propose that a 40% reduction in secretion of each TGF-β isoform in the TME should be sufficient to affect all major pathological features of *Zeb1*$^{i\Delta EC}$ tumors. Although TGF-β has been reported to function as an inhibitor of lymphangiogenesis (54, 55), we show here that impairing TGF-β signaling by vascular ZEB1 inactivation does not affect lymphatic vessel formation in tumors or lymph nodes. The mechanism causing this inconsistency is currently undefined and needs to be further investigated. Nevertheless, we demonstrate that vascular ZEB1 inactivation indeed reduces tumor lymphatic metastasis. As mentioned above, TGF-β is known to promote tumor cell invasion and metastasis by inducing the so-called EMT in tumor cells, a program that enables tumor cells to obtain migratory and invasive properties (that is, the tumor cells undergoing EMT are prone to metastasize to lymph nodes and other organs) (51–53). Based on the observations presented here, we propose that endothelial ZEB1 deletion impairs TGF-β expression and secretion to the TME and subsequently diminishes TGF-β activity in tumor cells in a paracrine fashion, thus reducing tumor cell metastasis to lymph nodes (via intact lymphatic vessels).

TGF-β together with VEGFA and ANG2 can elicit vascular abnormalities directly or indirectly (characterized by impaired blood perfusion and function), which hampers intratumoral infiltration of CD4$^+$ T cells, CD8$^+$ T cells, and specialized APCs such as tumor-associated dendritic cells and tumor-associated B cells (9, 34, 35, 39). Also, these 3 secreted signaling molecules can function as immunosuppressive cytokines in the TME, where they inhibit proliferation and effector function of tumor-infiltrating CD4$^+$ and CD8$^+$ T cells while diminishing antigen-presenting capacity and maturation/activation of specialized APCs. On the other hand, TGF-β is also known to activate *Foxp3* gene expression through enhanced binding of the SMAD2-induced transcription factor E2A to the *Foxp3* gene promoter in tumor-infiltrating CD4$^+$ T cells and thus promotes CD4$^+$Foxp3$^+$ Treg generation intratumorally, which restrains antitumor immunity (9, 41, 56–60). Here we provide evidence showing that inactivating vascular ZEB1 reduces expression and secretion of TGF-β, VEGFA, and ANG2 to the TME. We therefore propose that blocking the TGF-β/VEGFA-ANG2 pathway in *Zeb1*$^{i\Delta EC}$ tumor endothelium elicits tumor vessel normalization, which can facilitate intratumoral infiltration of CD4$^+$ and CD8$^+$ T cells and specialized APCs, thus provoking antitumor immunity (Figure 13I). Meanwhile, reducing the presence of TGF-βs (together with VEGFA-ANG2) in the TME results in enhanced proliferation and effector function of CD4$^+$ and CD8$^+$ T cells. On the other hand, diminishing TGF-β secretion to the TME severely impairs activation of *Foxp3* gene expression in CD4$^+$ T cells, which in turn reduces the proportion of CD4$^+$Foxp3$^+$ Treg subpopulation in CD4$^+$ T cells.

We unexpectedly find that vascular ZEB1 deletion increases the presence of activated CD4$^+$ and CD8$^+$ T cells but also induces PD-L1 expression in the LLC tumors, likely through activated T cell–derived cytokines (61–64). Targeting endothelial ZEB1 also profoundly increases tumor-infiltrating leukocytes (PD-L1 expression is predominant on tumor-infiltrating leukocytes but poorly expressed on LLC tumor cells or other cells in the TME), which consequently further increases PD-L1 expression in the tumors. Accumulating evidence has demonstrated that lack of response to anti–PD-1/PD-L1 treatment is associated with signature of TGF-β signaling in the TME, particularly in patients with immune-desert tumors (50). PD-1/PD-L1 and TGF-β (or VEGFA-ANG2) are key pathways with independent and complementary immunosuppressive functions (36, 37, 50), providing a rationale for dual targeting of PD-L1/PD-1 and TGF-β (or VEGFA-ANG2) pathways to treat solid tumors, especially immune-desert tumors. Indeed, recent reports have demonstrated that simultaneously blocking PD-L1/PD-1 and TGF-β (or VEGFA-ANG2) pathways by therapeutic anti-

bodies provokes robust and durable antitumor immunity and elicits tumor regression in various tumor models (36, 37, 50). The LLC tumors of *Zeb1*$^{i\Delta EC}$ mice exhibit reduced TGF-β (or VEGFA-ANG2) levels in tandem with upregulated PD-L1 level in the TME. Therefore, treatment with anti–PD-1 antibody can elicit tumor regression and markedly extend survival in LLC tumor–bearing *Zeb1*$^{i\Delta EC}$ mice, conferring long-term protective antitumor immunity. Further, durable presence of normalized well-functioning tumor blood vessels in *ZEB1*$^{i\Delta EC}$ tumors can facilitate therapeutic antibody perfusion to the tumor cores, achieving superior antitumor effect even used at low dose.

In conclusion, our findings demonstrate that tumor endothelium–derived ZEB1 plays a central role in regulating tumor growth and metastasis, tumor angiogenesis, vascular functionality and integrity, and antitumor immune response. Our evidence further suggests that targeting ZEB1 in combination with conventional chemotherapy or immune checkpoint blockade therapy may yield a potent and superior antitumor effect without eliciting systematic side effects.

Methods

Animals. The *Zeb1*^{flox} (*Zeb1*^{fl}) mice were generated and maintained in our laboratory. For generation of inducible EC-specific ZEB1-deleted mice, *Zeb1*$^{fl/fl}$ mice were crossed with *Cdh5(PAC)-Cre*^{ERT2} transgenics (28) (a gift from R.H. Adams, Max Planck Institute for Molecular Medicine and University of Münster, Münster, Germany). To induce Cre activity and vascular *Zeb1* inactivation in adult mice, 8-week-old mice were intraperitoneally injected with 1.0 mg tamoxifen (10 mg/mL in corn oil; T5648, Sigma-Aldrich) every other day for 2 consecutive weeks. To induce vascular *Zeb1* inactivation in pups, mice were treated with 0.1 mg tamoxifen at P3 and P6, and retinas were dissected at P7. All mice were on pure C57BL/6J background, and sex-matched littermate controls were used in all experiments.

Data availability. RNA-Seq data were deposited in the NCBI's Genomes Sequence Read Archive database (accession numbers SAMN13316576 and SAMN13316577).

Statistics. All data are presented as mean ± SD. Statistical analysis was carried out as described in each corresponding figure legend, and sample sizes are shown in each corresponding figure legend. Differences were evaluated between 2 groups by unpaired 2-sided Student's *t* test and between multiple groups by 1-way or 2-way ANOVA with Tukey's post hoc test. *P* less than 0.05 was considered statistically significant.

Study approval. All animal experiments were performed in accordance with protocols approved by the Animal Welfare and Ethics Committee of China Pharmaceutical University. The maximal tumor size permitted under the approved protocols is 3 cm (length) by 3 cm (width).

Detailed methods are provided in Supplemental Methods online. Primers used for PCR, qPCR, and ChIP assays are listed in Supplemental Table 1.

Author contributions

ZQW conceived the project, designed experiments, interpreted results, and wrote the manuscript. RF designed experiments, conducted experiments, and interpreted results. YL, NJ, and BXR conducted experiments with help from CZZ, LJL, WCL, HML, and ZYL. TL and SW provided relevant advice. RF, YL, NJ, and BXR share first authorship, and the order in which they are listed was determined by workload.

Acknowledgments

This research was supported by grants from the Natural Science Foundation of China (81973363, 81572745, 91539115, 81603134), Jiangsu Province Natural Science Funds for Distinguished Young Scholars (BK20170029), Jiangsu Province Natural Science Funds for Young Scholars (BK20160758), the Jiangsu Province Innovative Research Program, the State Key Laboratory of Natural Medicines of China Pharmaceutical University (SKLNMZZCX201808), and the Double First-Class University Project (CPU2018GF02). We thank R.H. Adams (Max Planck Institute for Molecular Medicine and University of Münster) for providing *Cdh5-Cre*^{ERT2} mice.

Address correspondence to: Zhao-Qiu Wu, State Key Laboratory of Natural Medicines and School of Basic Medicine and Clinical Pharmacy, China Pharmaceutical University, 639 Longmian Avenue, Nanjing 211198, China. Phone: 86.25.8618.5653; Email: zqwu@cpu.edu.cn.

1. Carmeliet P, Jain RK. Principles and mechanisms of vessel normalization for cancer and other angiogenic diseases. *Nat Rev Drug Discov*. 2011;10(6):417–427.
2. Hanahan D, Folkman J. Patterns and emerging mechanisms of the angiogenic switch during tumorigenesis. *Cell*. 1996;86(3):353–364.
3. Hanahan D, Weinberg RA. Hallmarks of cancer: the next generation. *Cell*. 2011;144(5):646–674.
4. Jain RK. Normalizing tumor microenvironment to treat cancer: bench to bedside to biomarkers. *J Clin Oncol*. 2013;31(17):2205–2218.
5. Jain RK. Normalization of tumor vasculature: an emerging concept in antiangiogenic therapy. *Science*. 2005;307(5706):58–62.
6. Jain RK. Antiangiogenesis strategies revisited: from starving tumors to alleviating hypoxia. *Cancer Cell*. 2014;26(5):605–622.
7. Sullivan R, Graham CH. Hypoxia-driven selection of the metastatic phenotype. *Cancer Metastasis Rev*. 2007;26(2):319–331.
8. Buckanovich RJ, et al. Endothelin B receptor mediates the endothelial barrier to T cell homing to tumors and disables immune therapy. *Nat Med*. 2008;14(1):28–36.
9. Fukumura D, Kloepper J, Amoozgar Z, Duda DG, Jain RK. Enhancing cancer immunotherapy using antiangiogenics: opportunities and challenges. *Nat Rev Clin Oncol*. 2018;15(5):325–340.
10. Cao Y, et al. Forty-year journey of angiogenesis translational research. *Sci Transl Med*. 2011;3(114):114rv3.
11. Ferrara N, Kerbel RS. Angiogenesis as a therapeutic target. *Nature*. 2005;438(7070):967–974.
12. Ebos JM, Lee CR, Cruz-Munoz W, Bjarnason GA, Christensen JG, Kerbel RS. Accelerated metastasis after short-term treatment with a potent inhibitor of tumor angiogenesis. *Cancer Cell*. 2009;15(3):232–239.
13. Ebos JM, Kerbel RS. Antiangiogenic therapy: impact on invasion, disease progression, and metastasis. *Nat Rev Clin Oncol*. 2011;8(4):210–221.
14. Pàez-Ribes M, et al. Antiangiogenic therapy elicits malignant progression of tumors to increased local invasion and distant metastasis. *Cancer Cell*. 2009;15(3):220–231.
15. Rivera LB, Bergers G. Tumor angiogenesis, from foe to friend. *Science*. 2015;349(6249):694–695.
16. Chen HX, Cleck JN. Adverse effects of anticancer agents that target the VEGF pathway. *Nat Rev Clin Oncol*. 2009;6(8):465–477.
17. D'Adamo DR, et al. Phase II study of doxorubicin and bevacizumab for patients with metastatic soft-tissue sarcomas. *J Clin Oncol*. 2005;23(28):7135–7142.
18. Kamba T, McDonald DM. Mechanisms of adverse effects of anti-VEGF therapy for cancer. *Br J Cancer*. 2007;96(12):1788–1795.
19. Krebs AM, et al. The EMT-activator Zeb1 is a key factor for cell plasticity and promotes

metastasis in pancreatic cancer. *Nat Cell Biol*. 2017;19(5):518–529.
20. Spaderna S, et al. The transcriptional repressor ZEB1 promotes metastasis and loss of cell polarity in cancer. *Cancer Res*. 2008;68(2):537–544.
21. Vandewalle C, Van Roy F, Berx G. The role of the ZEB family of transcription factors in development and disease. *Cell Mol Life Sci*. 2009;66(5):773–787.
22. Wellner U, et al. The EMT-activator ZEB1 promotes tumorigenicity by repressing stemness-inhibiting microRNAs. *Nat Cell Biol*. 2009;11(12):1487–1495.
23. Zhang P, et al. ATM-mediated stabilization of ZEB1 promotes DNA damage response and radioresistance through CHK1. *Nat Cell Biol*. 2014;16(9):864–875.
24. Bronsert P, et al. Prognostic significance of Zinc finger E-box binding homeobox 1 (ZEB1) expression in cancer cells and cancer-associated fibroblasts in pancreatic head cancer. *Surgery*. 2014;156(1):97–108.
25. Chaffer CL, et al. Poised chromatin at the ZEB1 promoter enables breast cancer cell plasticity and enhances tumorigenicity. *Cell*. 2013;154(1):61–74.
26. Soini Y, et al. Transcription factors zeb1, twist and snai1 in breast carcinoma. *BMC Cancer*. 2011;11:73.
27. Spaderna S, et al. A transient, EMT-linked loss of basement membranes indicates metastasis and poor survival in colorectal cancer. *Gastroenterology*. 2006;131(3):830–840.
28. Wang Y, et al. Ephrin-B2 controls VEGF-induced angiogenesis and lymphangiogenesis. *Nature*. 2010;465(7297):483–486.
29. Mazzone M, et al. Heterozygous deficiency of PHD2 restores tumor oxygenation and inhibits metastasis via endothelial normalization. *Cell*. 2009;136(5):839–851.
30. Catalano V, Turdo A, Di Franco S, Dieli F, Todaro M, Stassi G. Tumor and its microenvironment: a synergistic interplay. *Semin Cancer Biol*. 2013;23(6 pt B):522–532.
31. Swinson DE, Jones JL, Richardson D, Cox G, Edwards JG, O'Byrne KJ. Tumour necrosis is an independent prognostic marker in non-small cell lung cancer: correlation with biological variables. *Lung Cancer*. 2002;37(3):235–240.
32. Harris AL. Hypoxia—a key regulatory factor in tumour growth. *Nat Rev Cancer*. 2002;2(1):38–47.
33. Hamzah J, et al. Vascular normalization in Rgs5-deficient tumours promotes immune destruction. *Nature*. 2008;453(7193):410–414.
34. Lanitis E, Irving M, Coukos G. Targeting the tumor vasculature to enhance T cell activity. *Curr Opin Immunol*. 2015;33:55–63.
35. Tian L, et al. Mutual regulation of tumour vessel normalization and immunostimulatory reprogramming. *Nature*. 2017;544(7649):250–254.
36. Lan Y, et al. Enhanced preclinical antitumor activity of M7824, a bifunctional fusion protein simultaneously targeting PD-L1 and TGF-β. *Sci Transl Med*. 2018;10(424):eaan5488.
37. Schmittnaegel M, et al. Dual angiopoietin-2 and VEGFA inhibition elicits antitumor immunity that is enhanced by PD-1 checkpoint blockade. *Sci Transl Med*. 2017;9(385):eaak9670.
38. Cunha SI, Magnusson PU, Dejana E, Lampugnani MG. Deregulated TGF-β/BMP signaling in vascular malformations. *Circ Res*. 2017;121(8):981–999.
39. Liu J, et al. TGF-β blockade improves the distribution and efficacy of therapeutics in breast carcinoma by normalizing the tumor stroma. *Proc Natl Acad Sci U S A*. 2012;109(41):16618–16623.
40. Massagué J. TGFβ signalling in context. *Nat Rev Mol Cell Biol*. 2012;13(10):616–630.
41. Pickup M, Novitskiy S, Moses HL. The roles of TGFβ in the tumour microenvironment. *Nat Rev Cancer*. 2013;13(11):788–799.
42. Hsu DS, et al. Acetylation of Snail modulates the cytokinome of cancer cells to enhance the recruitment of macrophages. *Cancer Cell*. 2014;26(4):534–548.
43. Rembold M, et al. A conserved role for Snail as a potentiator of active transcription. *Genes Dev*. 2014;28(2):167–181.
44. Herranz N, et al. Polycomb complex 2 is required for E-cadherin repression by the Snail1 transcription factor. *Mol Cell Biol*. 2008;28(15):4772–4781.
45. Kim KJ, et al. Inhibition of vascular endothelial growth factor-induced angiogenesis suppresses tumour growth in vivo. *Nature*. 1993;362(6423):841–844.
46. Mazzieri R, et al. Targeting the ANG2/TIE2 axis inhibits tumor growth and metastasis by impairing angiogenesis and disabling rebounds of proangiogenic myeloid cells. *Cancer Cell*. 2011;19(4):512–526.
47. Goel S, Wong AH, Jain RK. Vascular normalization as a therapeutic strategy for malignant and nonmalignant disease. *Cold Spring Harb Perspect Med*. 2012;2(3):a006486.
48. Caramel J, Ligier M, Puisieux A. Pleiotropic roles for ZEB1 in cancer. *Cancer Res*. 2018;78(1):30–35.
49. Lazarova DL, Bordonaro M, Sartorelli AC. Transcriptional regulation of the vitamin D(3) receptor gene by ZEB. *Cell Growth Differ*. 2001;12(6):319–326.
50. Mariathasan S, et al. TGFβ attenuates tumour response to PD-L1 blockade by contributing to exclusion of T cells. *Nature*. 2018;554(7693):544–548.
51. Morikawa M, Derynck R, Miyazono K. TGF-β and the TGF-β family: context-dependent roles in cell and tissue physiology. *Cold Spring Harb Perspect Biol*. 2016;8(5):a021873.
52. Massagué J. TGFβ in cancer. *Cell*. 2008;134(2):215–230.
53. Hao Y, Baker D, Ten Dijke P. TGF-β-mediated epithelial-mesenchymal transition and cancer metastasis. *Int J Mol Sci*. 2019;20(11):E2767.
54. Oka M, et al. Inhibition of endogenous TGF-beta signaling enhances lymphangiogenesis. *Blood*. 2008;111(9):4571–4579.
55. Yan A, Avraham T, Zampell JC, Haviv YS, Weitman E, Mehrara BJ. Adipose-derived stem cells promote lymphangiogenesis in response to VEGF-C stimulation or TGF-β1 inhibition. *Future Oncol*. 2011;7(12):1457–1473.
56. Thomas DA, Massagué J. TGF-beta directly targets cytotoxic T cell functions during tumor evasion of immune surveillance. *Cancer Cell*. 2005;8(5):369–380.
57. Voron T, et al. VEGF-A modulates expression of inhibitory checkpoints on CD8+ T cells in tumors. *J Exp Med*. 2015;212(2):139–148.
58. Neuzillet C, et al. Targeting the TGFβ pathway for cancer therapy. *Pharmacol Ther*. 2015;147:22–31.
59. Akhurst RJ, Hata A. Targeting the TGFβ signalling pathway in disease. *Nat Rev Drug Discov*. 2012;11(10):790–811.
60. Maruyama T, et al. Control of the differentiation of regulatory T cells and T(H)17 cells by the DNA-binding inhibitor Id3. *Nat Immunol*. 2011;12(1):86–95.
61. Spranger S, et al. Up-regulation of PD-L1, IDO, and T_{regs} in the melanoma tumor microenvironment is driven by $CD8^+$ T cells. *Sci Transl Med*. 2013;5(200):200ra116.
62. Brown JA, et al. Blockade of programmed death-1 ligands on dendritic cells enhances T cell activation and cytokine production. *J Immunol*. 2003;170(3):1257–1266.
63. Zou W, Wolchok JD, Chen L. PD-L1 (B7-H1) and PD-1 pathway blockade for cancer therapy: mechanisms, response biomarkers, and combinations. *Sci Transl Med*. 2016;8(328):328rv4.
64. Chen L, Han X. Anti-PD-1/PD-L1 therapy of human cancer: past, present, and future. *J Clin Invest*. 2015;125(9):3384–3391.